A Study on the Effect of Bond Stress and Process Temperature on Palladium Coated Silver Wire Bonds on Aluminum Metallization

by

Jimy Jevers Gomes

A thesis
presented to the University of Waterloo
in fulfillment of the
thesis requirement for the degree of
Master of Applied Science
in
Mechanical Engineering

Waterloo, Ontario, Canada, 2015

Author's Declaration

I hereby declare that I am the sole author of this thesis. This is a true copy of the thesis, including any required final revisions, as accepted by my examiners.

I understand that my thesis may be made electronically available to the public.

– – – – – – – – –

Jimy Jevers Gomes

Abstract

In the past ten years, the increasing price of gold has motivated the wire bonding industry to look for alternative bonding wire materials in the field of microelectronics packaging. A new candidate wire to replace gold is palladium coated silver wire. In this thesis, the effect of the two specific process parameters “bond stress” and “process temperature” on the ball bonds made with the new candidate wire are investigated. Using 20 µm diameter wire and various level-combinations of these process parameter, ball bonds are produced according to a special accelerated optimization method to result in a target diameter of 46 ± 0.5 µm and target height of 16 ± 0.5 µm. Three different levels are used for each of the specific process parameters. After pre-selecting a few process parameters, the accelerated method determines the levels for the process parameters “impact force” and “electric flame-off current” with a 2×2 design of experiments. Then, the ultrasound parameter is maximized up to a level where a pre-selected ultrasonic deformation occurs to the bonds, maintaining the target bond diameter and height. The bond quality is measured by measuring the shear strength of the bonds. The results show that

- the bond geometry is not affected by the bond stress,
- the optimized specific process parameters vary by less than ~0.5 % when bond stress values are varied from 60 to 100 MPa,
- the variations in optimized parameters are larger than ~3.0 % when the BT is changed from 100 to 200 ºC,
- ball bonds achieve acceptable shear strength (> 120 MPa) when the values for both, bond stress and bond temperature, are high,
- ultrasound level and shear stress interact, the higher shear stress the lower the ultrasound level required.

An average shear strength of ~120 MPa is achieved with 11.4 % ultrasound, 100 MPa bond stress, and 200 ºC bond process temperature. In summary, a robust methodology is presented in this thesis to efficiently optimize the ball bonding process as demonstrated with the new candidate wire has a bondability similar to that of gold wire with only minor adjustment in the bonding process needed.

Acknowledgments

I would like to thank my supervisor, Dr. Michael Mayer for his continuous support and assistance during my stay as a graduate student. I was motivated to work hard and strive for my full potential under his supervision. I have achieved valuable skills which I believe will help me further my career goals.

Special acknowledgments goes out to Microbonds Inc. and Kulicke & Soffa Industries Inc. for providing valuable resources to make this project possible. Thanks to Natural Sciences and Engineering Research Council of Canada (NSERC), Ontario Centres of Excellence (OCE), and Initiative for Automotive Manufacturing Innovation (IAMI), ON, Canada, for assisting the project with fundings.

Finally, I would like to thank my family for their love and support. My successes in life would not be possible without their sacrifice.

Table of Contents

List of Figures

List of Tables

1. Introduction

Thermosonic wire bonding is the most popular interconnection method used in the microelectronics packaging industry [1]. Microelectronics packages protect the sensitive integrated circuits (ICs) from the outside environment by encapsulating them. In order for ICs to communicate with the outside world and be useful for various devices, electrical interconnection is required between the ICs and substrates. Thermosonic wire bonding is one of the methods that can provide this interconnection using fine wires which are bonded first on to metallized pads of the IC and then to the substrate terminals. The vast majority of ICs are interconnected using the wire bonding process [2].

Wire bonds can be either ball-wedge bonds or wedge-wedge bonds. In the case of ball-wedge bonding, ball bond (the first bond) is made between the wire and the metallization on the IC device, and wedge bond (the second bond) is made to the substrate that carries the IC. The bond pad material on the ICs is usually aluminum (Al) containing small amounts (< 1.0 %) of copper (Cu) and silicon (Si) dopants [2]. The substrate pad materials can be silver (Ag), gold (Au), or copper (Cu). The ICs are usually die-attached to the substrate with adhesive epoxy.

Gold (Au) is the most used bonding wire material in the thermosonic wire bonding process. High electrical conductivity, low hardness, high malleability, and absence of surface oxide make Au the least complicated and most suitable to use in wire bonding. However, the price of Au has increased to five-folds in the past years, and reached a record high of $63.50 per gram ($1800.00 per ounce) in 2012 [3]. The high cost of Au has motivated the wire bonding industry to look for alternative bonding wire materials.

As of 2012, the most popular alternative to Au is Cu and palladium (Pd) coated Cu (PCC). For example, Texas Instruments produced ~6.5 billion units of analog, embedded processors, and wireless products using Cu wire bonding technology in May 2012 [2]. Besides lower cost, Cu has superior electrical conductivity and higher tensile strength (221 to 455 MPa [4]) which helps in producing straighter wire loops. However, the higher hardness of Cu (Vickers hardness of 369 MPa compared to 216 MPa of Au [5]) usually requires for higher levels of force and ultrasound required during bonding which in turn makes the ICs susceptible to underpad damage. Fur-

thermore, pure Cu wire has poor shelf-life since it oxidizes readily in the air. Shielding gas is required for Cu wire bonding to prevent in-process oxidation which is a recurring cost added to the bonding process.

The drawbacks of Cu wire makes Ag a more favorable alternative to Au since the material properties of Au and Ag are quite similar. However, bonds made with pure Ag wire on Al bond pads degrade fast during thermal aging and corrode easily under humid condition [6,7]. Alloying pure Ag with Au and Pd tends to improve the reliability performance of the Ag wires [8-11]. In particular, the presence of Pd reduces the growth rate of the intermetallics (IMCs) at the bond interface and contributes to the longer bond life [7,12-14].

The addition of Pd and Au as alloying elements reduces the electrical conductivity and increases the hardness of the Ag wire. In addition, the cost of alloying increases the production cost of the Ag wires. An alternate method to add Pd into Ag-Al bond interface is to use the Pd coated Ag (PCS) wires as produced exclusively by Microbonds Inc., Markham, Ontario.

Pure Ag wire coated with 90 to 120 nm thick Pd on the surface uses less amount of Pd than the alloyed wires and preserves the high electrical conductivity and good formability of the pure Ag wire. One study has shown that PCS wire requires no shielding gas to form good quality free air ball (FAB) [15]. However, a detailed study on the PCS wire bonding process has not been reported. More research is necessary to understand this novel wire material if it were to be accepted by the wire bonding industry for volume production.

1.1. Objective

The objective of this study is to investigate the effects of bond stress and process temperature on the PCS ball bonds. The ball bonds are optimized for specific target geometry and mechanical strength using the accelerated optimization method [16] developed further in this thesis. Optimization is done at different combination of bond stress and process temperature. The optimal process condition for PCS ball bonds are identified from the results. The wedge bond process is not investigated in this study.

1.2. Thesis Outline

The thesis is divided into six chapters. Chapter 1 includes the introduction and the objectives of this study. Chapter 2 provides background information on the thermosonic wire bonding process, suitability of Ag as bonding wire material, bond quality assessment techniques, and ball bond optimization method used to achieve the objectives of this study. Chapter 3 contains the detail of the experimental procedure which includes the preparation and design of experiments (DOE). The results of the experiments are given in Chapter 4. Chapter 5 discusses the results and identifies the optimized bonding conditions for the PCS ball bonds. Conclusions and outlook are given in Chapter 6.

2. Literature Review

2.1. Thermosonic Wire Bonding Mechanism

Thermosonic wire bonding uses heat, normal force, and ultrasonic energy to make wire bonds. It is a solid-state bonding process where no melting occurs during bonding [1]. Metallic bonds are formed where intimate contact is achieved between the two materials to be joined at the atomic level. Fig. 2.1 shows example of thermosonic ball-wedge and wedge-wedge bonds.

A typical thermosonic ball bonding process steps are illustrated in Fig. 2.2. The first step of the ball bonding process is the electric flame-off (EFO) process. During EFO, a high electrical potential is applied between the electrode and the wire tail suspending from the capillary. This results in an electrical discharge (or spark) with a high enough energy to melt the tip of the wire tail. The molten metal rolls up in to a spherical ball due to surface tension where it then solidifies instantly once the spark current is turned off. This ball is called the free air ball (FAB).

After EFO, the wire clamp is opened and the capillary moves downward towards the IC device, which is typically heated to a temperature above 150 ºC. The capillary presses the now solid FAB onto the bond pad with an impact force (IF), deforming it to almost its final shape in what is called an impact deformation process [17,18]. The deformed ball is then held in place for a certain amount of time with a bond force (BF) which is low enough to ensure that no major additional ball deformation takes place. During this time, a transducer applies ultrasonic (US) energy to the capillary tip, creates vibration, and generates friction between two material surfaces. The combination of heat, force, and frictional energy creates a solid state bond and sometimes results in some minor additional deformation called ultrasound enhanced deformation (UED) [19,20].

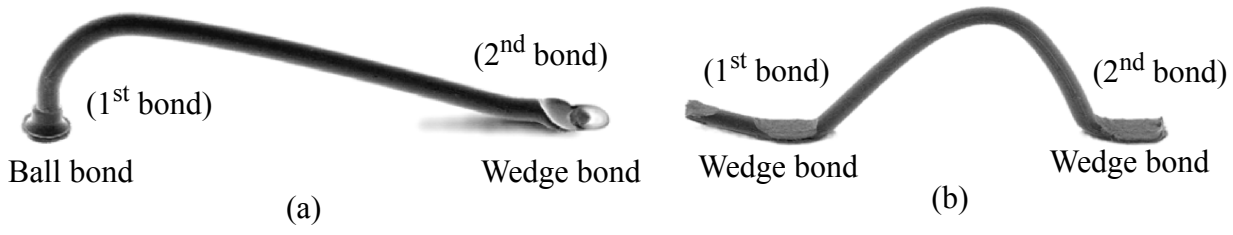

Fig. 2.1 Side view of a (a) ball-wedge bond and (b) wedge-wedge bond. Reproduced from [19].

The clamp holding the wire then opens and the capillary moves to the location of the second bond while the wire is fed through. The capillary presses the looped wire onto the bond pad of the package (terminal), and makes the wedge bond (also known as crescent bond) using similar values of heat, force, and ultrasonic energy.

The capillary and the open clamp then move upwards by a certain distance, feeding out a defined length of wire before stopping. The clamp closes, preventing any more wire from feeding through the capillary. The capillary and clamp then move upwards again, causing the wire to break at its weakest point which is located where the wire is pinched after the second bond location [1]. This leaves a wire tail hanging with a definite length from the capillary which is available for formation of the FAB of the subsequent bonds.

Thermosonic wire bonding is a very fast process. For example, the ESEC 3088 automatic ball-wedge bonder (Fig. 2.3) used in this study can produce 10 bonds per second.

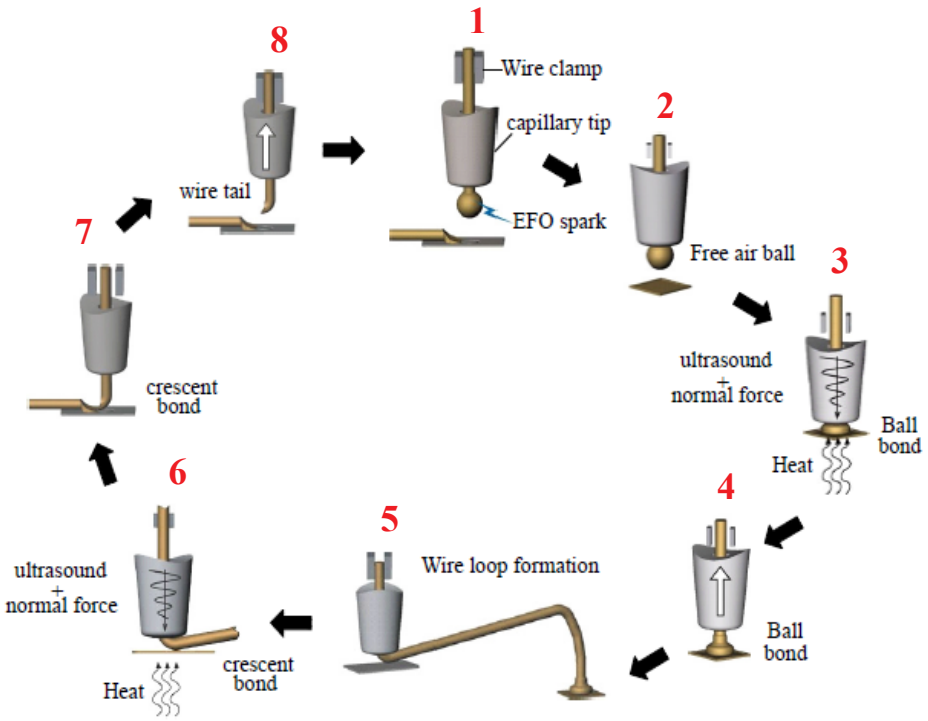

Fig. 2.2 Schematic showing the thermosonic ball-wedge bonding process [21].

2.2. Important Process Parameters for Ball Bond

Several process parameters are important for the production of a ball bond of desired shape with optimized strength. The most important parameters for successful and high quality bonding are initial FAB diameter, normal forces (IF and BF), US, and substrate temperature (or bond temperature, BT).

A standard method of ball bonding involves FAB deformation using IF before the ultrasonic bonding begins and is known as the impact deformation process. Another method of ball deformation combines force and ultrasound in a process called ultrasound enhanced deformation (UED). A typical ball bond produced using impact deformation process is shown in Fig. 2.4 Normally, a process is a mixture of the two methods.

For the impact deformation process, the final bonded ball geometry, defined by the bonded ball diameter and the bond height, (Fig. 2.4b), is a product of the IF and the FAB diameter. The FAB diameter in turn is determined by the EFO current (I_{EFO}), wire tail length (TL), and the EFO time (t_{EFO}). Usually the TL is held constant because of its limited influence on the result. Only the I_{EFO} and t_{EFO} are modified to vary FAB size.

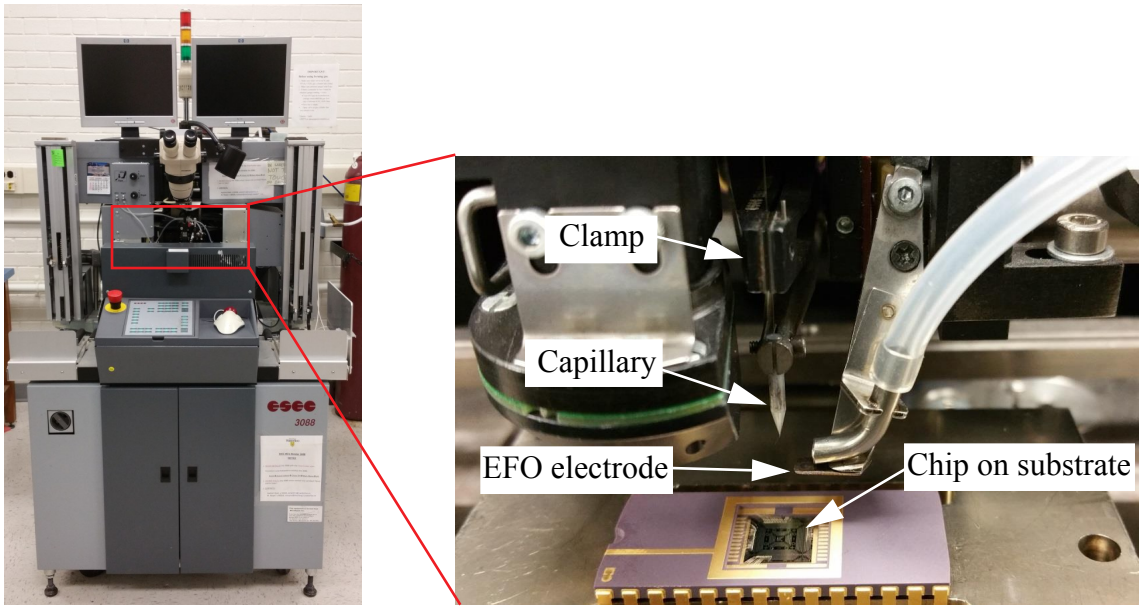

(a) (b)

Fig. 2.3 Photograph of (a) ESEC 3088 automatic ball-wedge bonder with (b) close up of bondhead indicating capillary, clamp, and EFO electrode.

The bond strength for a given geometry is measured as shear strength (SS) using a shear testing machine. SS depends on BT and US which is varied to achieve the peak strength. BT is one of the most important parameters for bond SS. Typically, bonds are made at temperatures of at least 150 ºC in order to ensure formation of a strong bond. BT cannot be too large because of temperature limits of materials involved, especially when polymer substrates are used. Once EFO parameters, normal forces and BT are established for a target geometry, the bond strength is usually maximized by varying the US [16]. Bond time (Bt) is typically fixed at standard values between 10 and 20 ms, and are not varied between processes. Generally speaking, a low Bt value can be compensated with a high US value and vice versa. Bt therefore is chosen low if high productivity is desired and subsequent optimization turns out a relatively high US value. For a more robust process, a higher Bt value combined with a lower US value can be attempted. A schematic shown in Fig. 2.5 summarizes the important wire bonding process parameters.

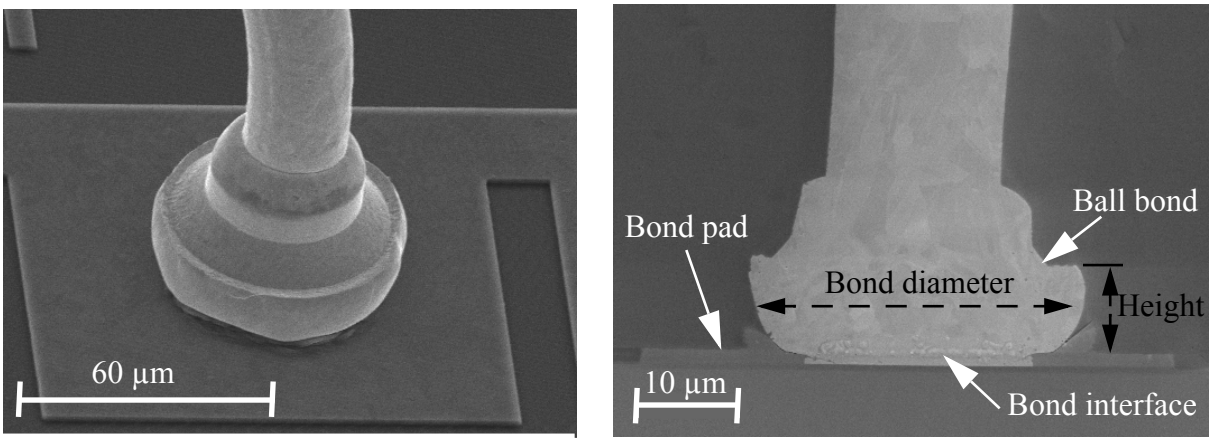

(a) (b)

Fig. 2.4 SEM images of typical ball bonds from (a) isometric view, (b) cross-sectional view. The isometric view in (a) is of 56 µm dia. ball bonds produced using 25 µm Au wire. The cross-sectional view in (b) is of 32 µm dia. ball bonds produced using 18 µm dia. PCS wire. Fig. 2.4b is reproduced from [22].

2.3. Silver as Bonding Wire Material

Typical bond wires are usually 99 % (refereed as ‘2N’) or 99.99 % (refereed as ‘4N’) pure. The remaining wire composition includes various dopants in order to increase the mechanical properties of the wire [2]. Dopant levels are usually kept at a minimum because most dopants reduce the conductivity of the wires which is undesirable.

Pure Ag has the highest electrical conductivity among all metals [23]. The hardness of pure Ag (251 MPa) is close to that of Au (216 MPa) [5]. Ag wire is very similar to Au wire in terms of bondability [3,6,15,23]. However, pure Ag is not favorable to be used as bonding wire because the Ag-Al IMCs forming at the bond interface degrade fast during thermal aging [6] and corrode easily under humid environment [7]. In addition, pure Ag does not form good quality FAB consistently, which is well-known from the field experience.

Ag wire alloyed with Au and Pd has reported to improve the bondability and reliability performance of the wire. In the case of Au wire, Pd addition to results in formation of a Pd rich barrier layer on top of the IMCs and retards the Au IMC inter-diffusion, thus enhances the high tempera-

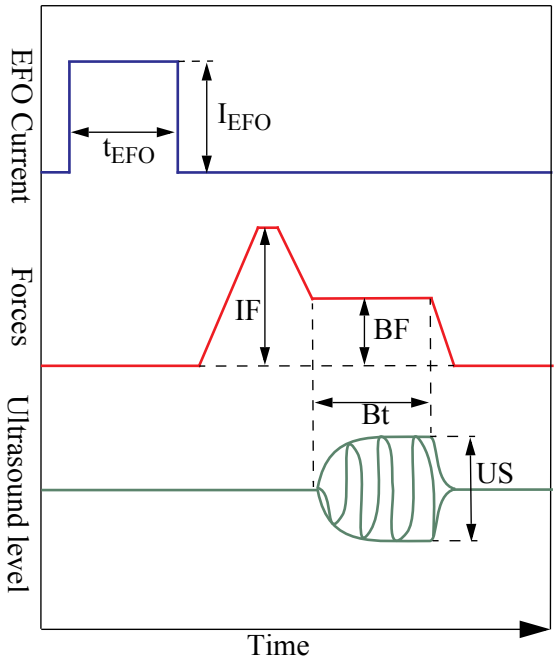

Fig. 2.5 Profiles of important parameters for thermosonic wire bonding process. Reproduced from [16].

ture storage (HTS) reliability performance [24]. Addition of Pd to Ag wire is found to have positive effects as well [8-11].

It is reported that Ag wire alloyed with 3 wt.% Pd has prolonged life in pressure cooker testing (175 ºC temperature and 100 % relative humidity) compare to "4N" Ag wire [7]. According to [7], Pd forms a very thin palladium-oxide (PdO) layer outside the Ag wire. This thin layer of oxide works as a passivation layer and prevents Ag from diffusing out of the bonded area. The growth rate of Ag-Al IMCs decreases and Al bond pad displays slower corrosion. However, diffusion of Ag is effectively inhibited only when Pd addition is more than 20 wt.% [25].

Alloying the wire with high amount of Pd increases the overall resistivity and increases the production cost of the wire. An alternate way to introduce more Pd into the bond interface without sacrificing the benefits of Ag wire is to use the Pd coated Ag (PCS) wires. Fig. 2.6 shows the color difference between a spool of PCS and Au wire. Pd coating solves another inherent problem that exists in pure Ag wires. Pure Ag oxidizes in air, hence, protective shielding gas environment is required for FAB formation. One study shows that high quality FABs can be formed in atmospheric condition with PCS wires [15]. Thus, PCS wires promise to be better suited to wire bonding industry than alloyed Ag wires. However, more work is required to demonstrate the improved bondability and reliability of Pd coated Ag wire, and its suitability for wire bonding in mass production.

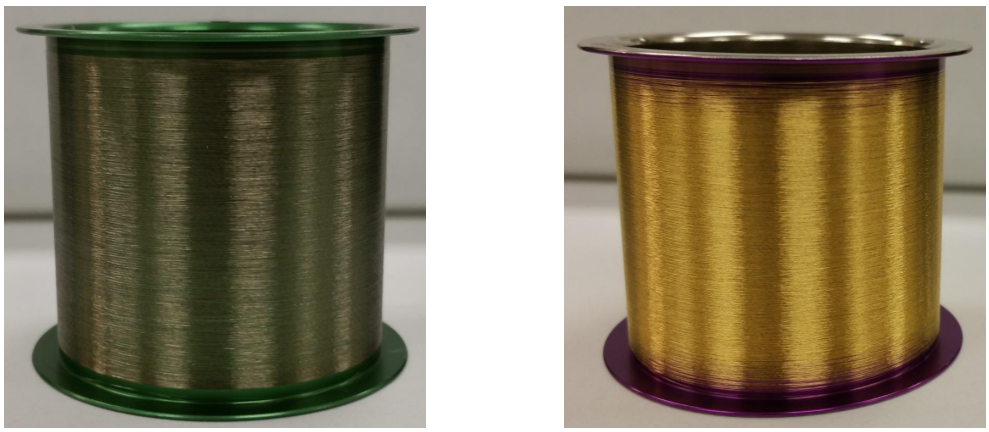

(a) (b)

Fig. 2.6 Photograph of 20 µm (a) PCS and (b) Au wire spool.

2.4. Bond Quality Assessment

The conventional techniques used to evaluate the wire bond quality are visual inspection (optical and electron microscopy), pull testing, and shear testing. Most of the traditional quality assessment methods are destructive (except the visual inspection). Often the methods are manual, tedious, and time consuming.

2.4.1. Pull Test

The pull test is a destructive method of bond strength evaluation in which a hook is placed under the wire loop, and pulls the wire upwards until failure occurs (Fig. 2.7). The pull force exerted is measured and indicates bond strength. In order to measure the strength of the wedge bond, the hook is located towards the middle of the loop. To measure the strength of the ball bond the hook is located as close to the ball as possible for a vertical pull direction.

While the pull force is an excellent indicator of wedge bond strength, it is not always ideal for evaluating ball bonds. If a minimum of 10 to 20 % of the interface is bonded [1], failure will occur at the heat affected zone (HAZ) of the ball neck rather than at the pad interface during pull test due to the large interfacial area of the ball bond. Thus, little information is gained with the pull test on the ball bond interfacial strength. Destructive wire pull testing is governed by the MIL-STD-883E standard [26].

2.4.2. Shear Test

Shear testing is a destructive test that quantifies the strength of the ball bond at the interface

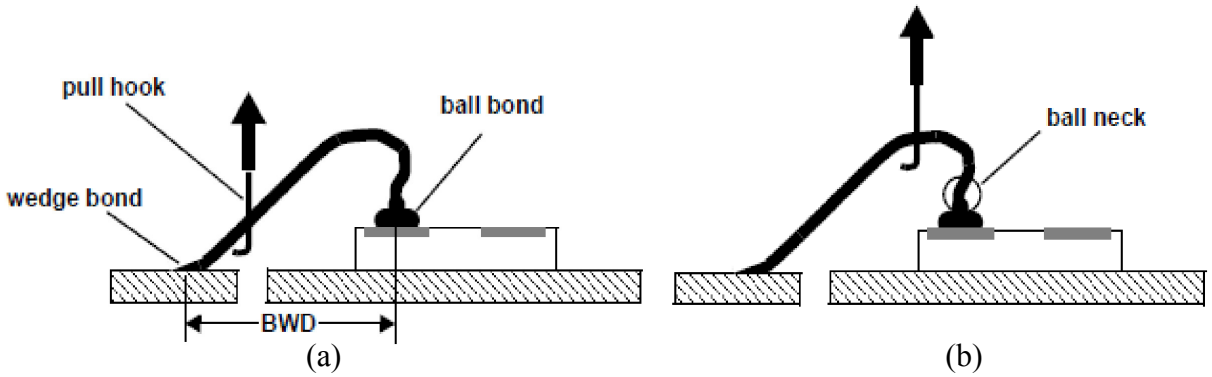

Fig. 2.7 Schematic showing pull force testing for (a) wedge bond and (b) neck or HAZ breaking force for ball bond. Reproduced from [28].

between the bonded ball and pad metallization. A shear tool applies tangential force to the ball bond and measures the shear force (SF) at failure as illustrated in Fig. 2.8. The shear force is then divided by the bonded area to calculate the shear stress (SS) which is often given in units of gf/mil^2 (1 gf/mil^2 is equal to 15.2 MPa). Since the bonded area is difficult to measure directly, the ball diameter at capillary imprint (BDC) where the capillary makes contact to the top of the ball during bonding is often used to estimate the bonded area (shown in Fig. 2.8). SS values are calculated using Eqn. 2-1 to make the bond strengths between different bonds comparable.

$$SS = \frac{SF}{\pi \times (BDC/2)^2} \tag{2-1}$$

For a proper shear test the bottom of the shear tool should maintain a specific shear height (SH) from the pad surface, approximately between 1/4 and 1/3 of BH. In the shear testing there are many different failure modes. The most common being interfacial shear, ball shear, and cratering. Interfacial shear is undesirable which often indicates poor bonding process or excessive intermetallic growth. Ball shear indicates that the bond is stronger than the wire material itself. The destructive shear testing method is governed by the JEDEC standard of JESD22-B116A [27].

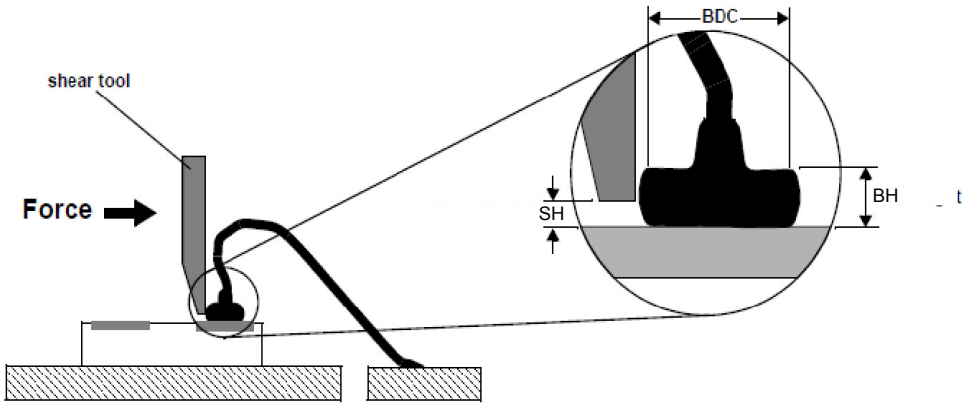

Fig. 2.8 Schematic showing shear testing of ball bonds. Reproduced from [28].

2.5. Ball Bond Optimization Method

Several process setup tasks are required before any mass production with new bonding wire can be started. In general, the wire bondability is established by proper selection of equipment, materials, and process. One of the demanding process setup tasks is ball bond optimization. The quality of optimized ball bonds vary less between samples which results in a robust and consistent process.

Optimization methods can include simple trial and error, design of experiment (DOE) [29], response surface methodology (RSM) [30], and numerical finite element analysis (FEA) [31]. For example, a sequence of tests is carried out in [32] to optimize ball bond quality, starting with variable selection using an analysis of variance (ANOVA), followed by screening experiments, a fractional factorial DOE to find the detailed ranking of the process factors, and finally a central composite type DOE combined with the response surface method to find process windows for the main factors. Such a stepwise approach has excellent results but requires substantial effort, and the adjustment of the geometry of the bonded balls are not considered.

More recent attempts to optimize the wire bonding process parameters are reported in [33,34]. In [33], an experimental design and grey relational analysis (GRA) is used to identify the relationship between process parameters and responses first, and then parameters are optimized using a fuzzy inference system and Taguchi method. The method provides superior optimization performance, however, it is a complex method requiring detail understanding of the process steps and the method did not focus on optimizing the bonded ball diameter. GRA is also used in [34] where an integrated neural network and genetic algorithm method is applied to achieve optimized parameters. Optimized parameters are then verified experimentally using RSM and excellent results are achieved. The method, however, is long and complex, and requires substantial amount of time and statistical understanding.

An accelerated ball bond optimization method is used for this study which is reported in [35]. The method uses the impact deformation process and separates the bond geometry formation step from the strength maximization step. The method only optimizes the IF, I_{EFO} (or alternatively t_{EFO}), and US parameter. The optimization method is performed once the BT and BF are selected.

In this method, effective stress on the ball bond during bond formation is quantified by dividing the BF value with the cross-sectional area of the bond which is measured by BDC. An effective normal stress (σ_N) induced on the ball bonds by the bond force (BF) during bond formation is defined using Eqn. 2-2. The σ_N value is independent of bond geometry which makes the BF values obtained from the literature comparable. Acceptable bond strength and reduction of underpad stress can be obtained with σ_N of 70 to 75 MPa for Au wire and ~90 MPa for Cu wire [37].

$$\sigma_N = \frac{BF}{\pi \times (BDC/2)^2} \tag{2-2}$$

The accelerated optimization is fast and can be performed with a minimal amount of sample. For example, only 110 wire bonds were used to complete the optimization in 220 min for 25 µm Au wire [35]. In addition, the method is flexible since each steps in optimization process can be repeated and verified easily.

3. Experimental

3.1. Preparations

The bonding experiments are carried out on an ESEC 3088 automatic wire bonder (Besi, Cham, Switzerland), a type of wire bonder presented in 1999 for the first time that has the ability to bond 60 micron pitch balls under production conditions which was considered “ultra fine pitch” at the time of introduction [38]. The capillary used is a commercial ceramic bottleneck capillary having a hole diameter of 27.2 ± 0.33 µm and a chamfer diameter of 37.18 ± 0.44 µm. The wire used is a 20 µm diameter Pd coated Ag (PCS) wire. Table 3.1 shows the resistivity values measured for different bond wire materials. Pure Ag and PCS wire have the lowest resistivity among the bonding wires.

Test chips used for the bonding process are typically 2.5 mm by 2.5 mm and 0.5 mm thick. The test chips are die attached to PLCC44 leadframes using a standard die attach method involving Ag filled epoxy to glue the chip in place, which is then cured in an oven at 175 ºC for 3 h. An example of the test chip mounted on the PLCC44 leadframe and wire bonded with the PCS wire is shown in Fig. 3.1. The bonding pads for the ball bonds are made of standard bond pad Al containing 0.5 % Cu dopant and are ~2.3 µm thick on average (Fig. 3.2). A total of 56 bond pads are used per test chip. The wedge bonds are made on the Ag metallized substrate as shown in the example micrograph in Fig. 3.3.

Ball bonds are optimized for a target diameter of 46 ± 0.5 µm. A minimum space of 3 µm is left between the bond periphery and the outside border of the pad to verify bond centering. Bonded

Table 3.1 Measured resistivity of different bond wire materials

Wire Material	Wire Diameter [µm]	Resistivity [nΩm]
Au (99.99 %)	25	26.2
Ag (99.99 %)	25	17.2
Ag alloy	25	52.3
Uncoated Ag (99.99 %)	20	17.3
Pd coated Ag	20	17.0

ball diameter at capillary imprint (BDC) is considered equivalent to the bond diameter. BDC is measured in the *x* and *y* directions using optical micrograph as shown in Fig. 3.4a, and the average of the measurements is taken.

Bond height (BH) to BDC ratio of 1:2.8 is found to be reliable for Au wire bonds [35]. Hence, the target BH chosen for this study is 16 ± 0.5 µm. BH is measured from the change required to focus on the bottom and top of the ball bond (Fig. 3.4a and b).

Bond shear strength is determined from shear force (SF) and BDC values using Eqn. 2-1. A SS of unaged Au wire (120 MPa) is considered acceptable [36]. A shear tool height of 4 µm is used to

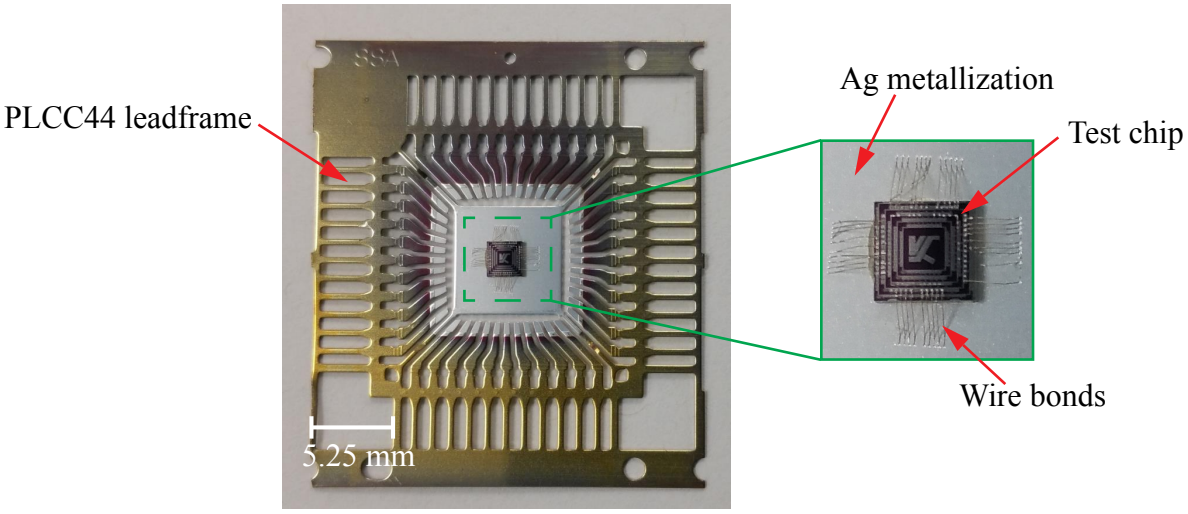

Fig. 3.1 Picture of a wire bonding test chip mounted on a substrate. Only one unit of the eight units on the PLCC44 leadframe strip is shown. The test chip is 2.5 × 2.5 mm and 0.5 mm thick.

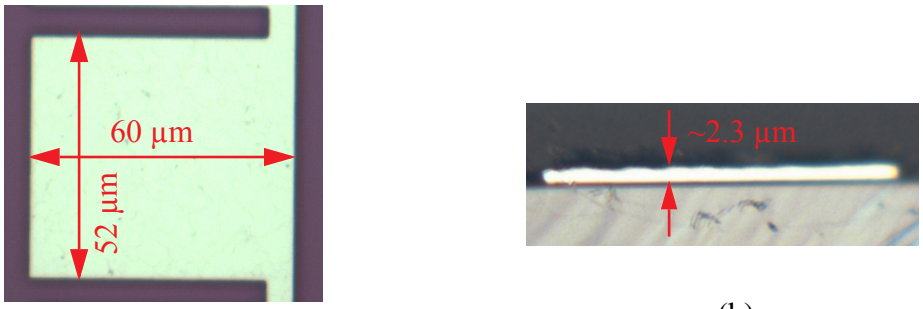

(a) (b)

Fig. 3.2 Micrographs of a typical ball bond pad, (a) top view with dimensions and (b) cross section showing pad thickness. The adjacent pad centers are 60 µm apart.

measure the SF value of each bond.

The wedge bond parameters are not fully optimized for and are identified by trial-and-error for this study. In order to be acceptable, the wedge bond should always stick to the material and no fish-tailing (peeling) should be observed. Acceptable wedge bonds are achieved with the bond parameters given in Table 3.2 at the lowest BT of 100 ºC. Five test bonds are made for each combination of parameters to carry out the experiment. A total of 450 bonds are used to complete the study.

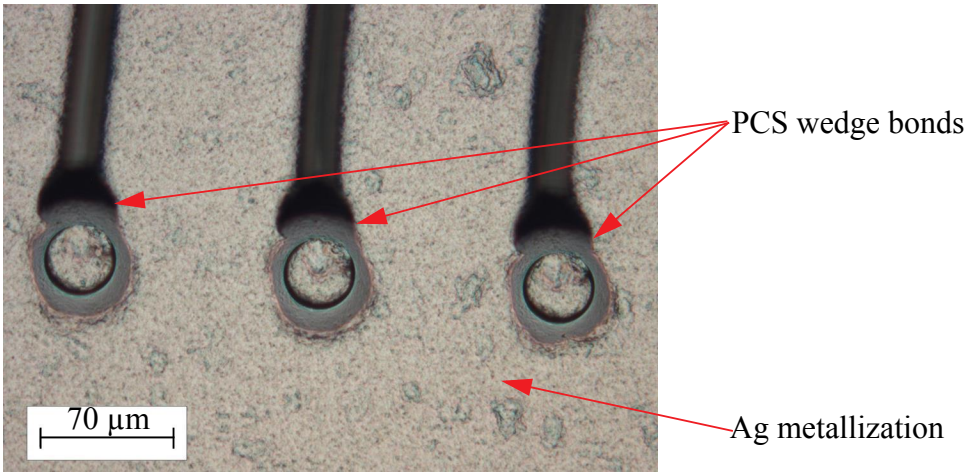

Fig. 3.3 Example micrograph of typical PCS wedge bonds made on Ag metallization.

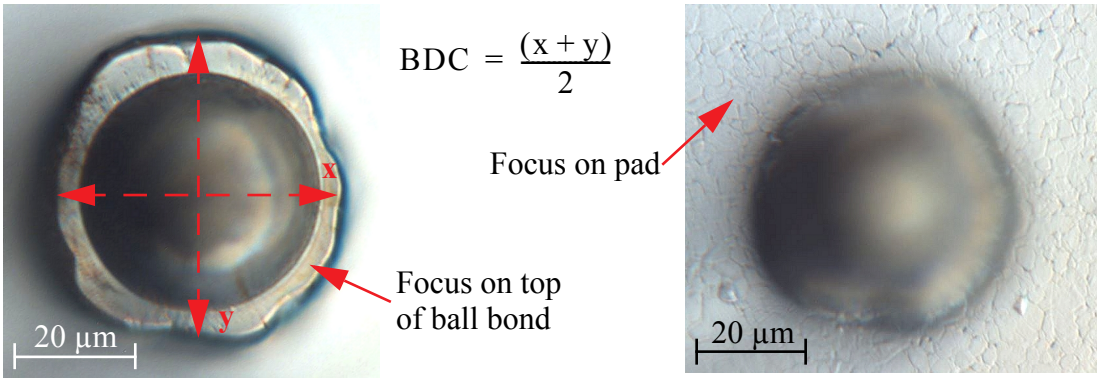

Fig. 3.4 Example micrograph of a typical PCS ball bond, (a) focus on top for BDC measurement, and, (b) focus on the pad for BH measurement.

The complete experimental procedure for the ball bond process optimization is outlined in a compact block diagram in Fig. 3.5 to give a simplified overview of the main components. The details of each step are discussed in this and the following subsections. Three key bond parameters, IF, I_{EFO}, and US, are optimized in this study. The other bond parameters are selected from literature and field experience, and given in Table 3.2.

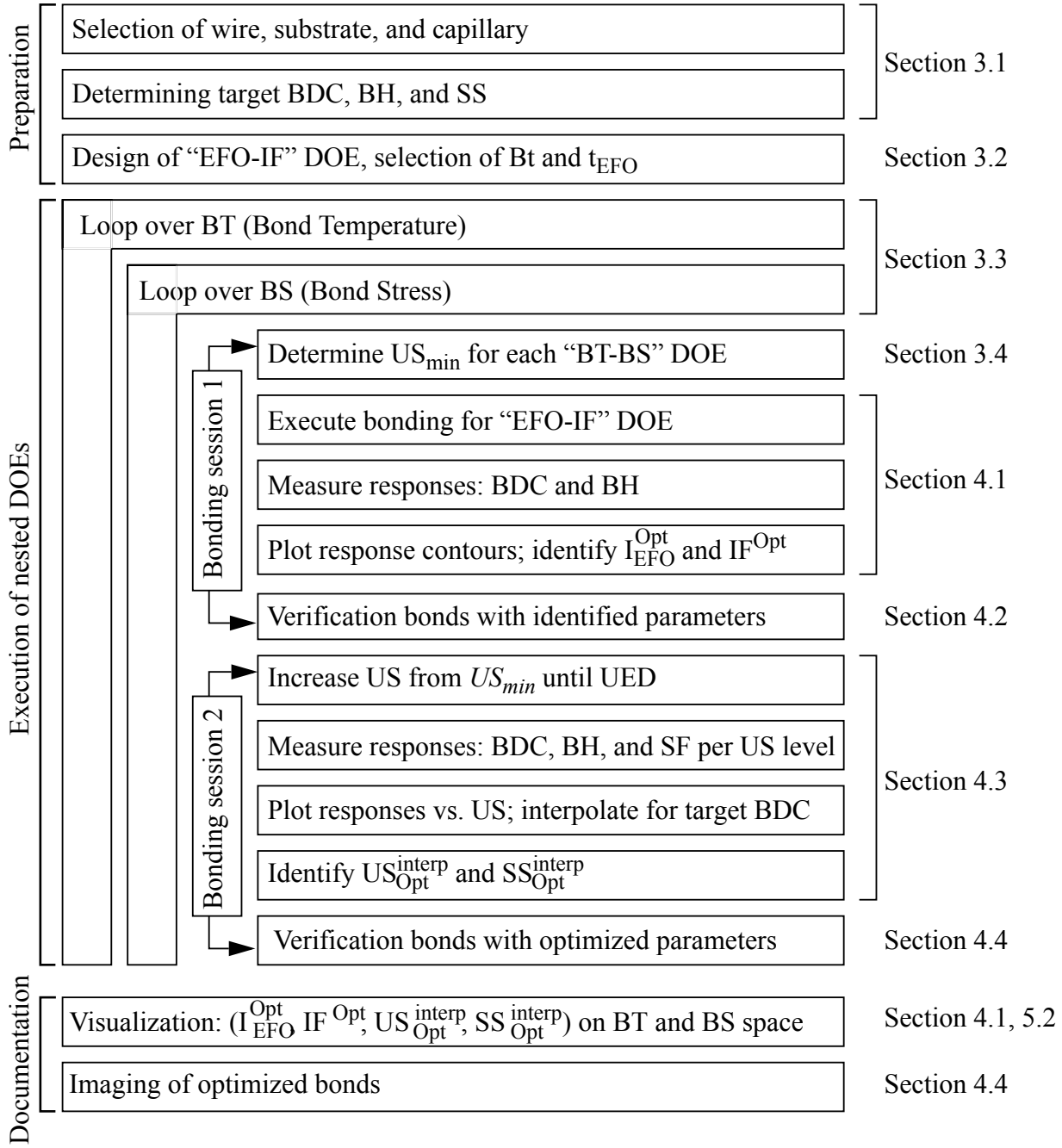

Fig. 3.5 Block diagram detailing the sequence of steps for experiments.

In addition, a flow diagram of the procedure is shown in Fig. 3.6 to also visualize conditional bifurcations in the procedure.

3.2. Design of "EFO-IF" DOE

A 2×2 full factorial experiment is used to obtain the target bond geometry. The two factors of the factorial experiments are IF and I_{EFO}, and the response of interests are the resultant BDC and BH. Other EFO parameters including the EFO time (t_{EFO}) is kept constant during the experiment. Since the factorial experiment optimizes the I_{EFO} and IF for the target geometry, it is referred as "EFO-IF" DOE in subsequent sections.

The IF values chosen for the DOE are 350 and 500 mN. The range of the IF is selected based on the following considerations: consistent BDC is not observed on the bonds for IF < 350 mN indicating a minimum level for IF, and bonds are severely deformed (or squashed) when IF > 500 mN is used for any combination of σ_N and BT. The range for I_{EFO} is chosen to be 60 and 70 mA. The highest I_{EFO} level of the bonder is 70 mA and circular FABs do not form with the PCS wire when I_{EFO} < 60 mA. Bonder microscope is used to verify the formation of adequate FAB size.

Table 3.2 Bond parameters used to start bonding experiment

	Parameters	**Values**		
Wedge Bond	Impact Force (IF) [mN]	300		
	Bond Force (BF) [mN]	200		
	Bond Time (Bt) [ms]	20		
	Ultrasonic Power (US) [%]	25.14		
EFO	EFO Time (t_{EFO}) [ms]	0.20		
	Elec-wire Dist. (EWD) [µm]	200		
	Tail Length (TL) [µm]	500		
	EFO Current (I_{EFO}) [mA]	To be optimized		
Ball Bond	Bond Force (BF) [mN]	100	133	166
	Bond Time (Bt) [ms]	20		
	Impact Force (IF) [mN]	To be optimized		
	Ultrasonic Power (US) [%]	To be optimized		
	Bond Temperature [ºC]	100	150	200

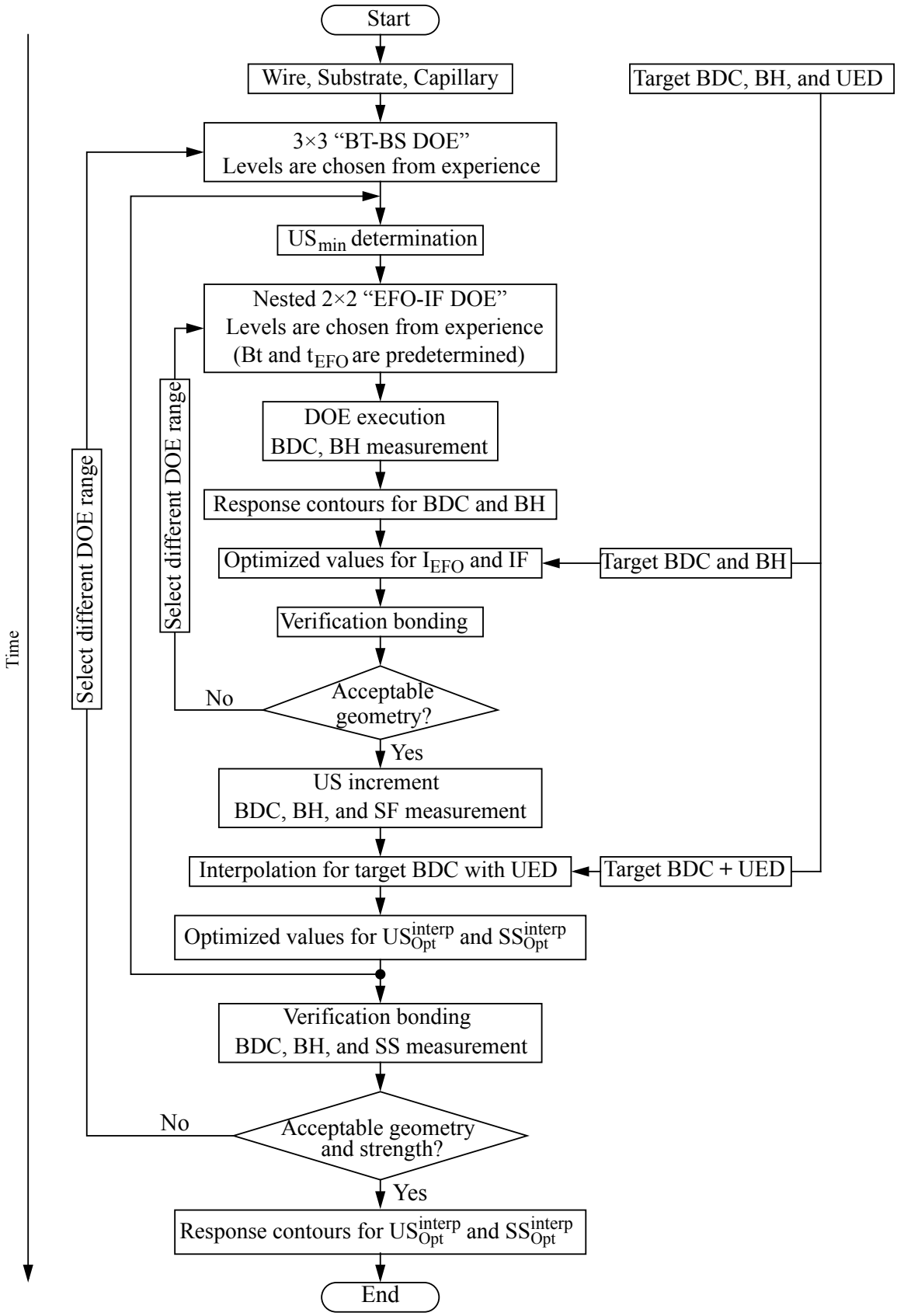

Fig. 3.6 Flow diagram showing the experimental steps against a time axis.

3.3. Design of "BT-BS" DOE

A 3×3 factorial experiment is used to determine the effect of bond force and temperature on ball bonds. The two factors used are bond stress (σ_N) and process temperature (BT). Bond stress is used instead of BF because it is independent of bond geometry. This full factorial experiment is referred as "BT-BS" DOE in subsequent sections.

Three different levels of σ_N used for the experiment are 60, 80, and 100 MPa. Using the target BDC value of 46 µm in Eqn. 2-2, the corresponding BF values are calculated to be 100, 133, and 166 mN, respectively. The three BT values used are 100, 150, and 200 ºC. The range of values for both σ_N and BT are chosen to be large enough to obtain significant variation in responses.

3.4. Identification of US_{min}

It is desired to minimize or even prevent ultrasound enhanced deformation (UED) during bond geometry formation to manage the complexity of the optimization task. Therefore, the EFO-IF DOE is performed at minimal US levels that still result in most of the balls sticking to the pads. Preventive non-stick on pad (NSOP) behavior is observed below this US level (US_{min}). Test bonds for each set of parameters are made at constantly decreasing US until some of the ball bonds no longer stick to the bond pad. At this point, the US is increased by 1 % to a level where no NSOPs are observed. The US value is represented using "%" which indicates the fraction of the full ultrasound amplitude available. US_{min} depends on BT. US_{min} is higher when BT is lower. The US_{min} values used in this experiment for three different BT are given in Table 3.3.

Table 3.3 US_{min} values used for the bond geometry optimization

Bond Temperature [BT]	Ultrasonic Power [%]
100 ºC	12.09
150 ºC	11.14
200 ºC	10.01

4. Results

4.1. Bond Geometry Optimization

The EFO-IF DOE is executed for each combination of σ_N and BT. In the EFO-IF DOE, test bonds are made for each combination of IF and I_{EFO}, and the BDC and BH are measured. Contour plots are constructed with the average values of BDC and BH by plotting them against IF and I_{EFO}. An example contour plot is shown in Fig. 4.1 based on the data given in Table 4.1 which is used to optimize the geometry for σ_N = 80 MPa and BT = 100 ºC. The isolines for constant BDC and BH values are intersecting one another. The intersection point of the isolines for target BDC (46 µm) and BH (16 µm) gives the optimized IF (IF^{Opt} = 401.37 MPa) and I_{EFO} (I_{EFO}^{Opt} = 68.10 mA) values. The MATLAB script used to generate the contour plots and calculate the optimized parameters is given in Appendix A.

The I_{EFO}^{Opt} and IF^{Opt} values extracted from the contour plots for each σ_N and BT combination are shown in Fig. 4.2 and Fig. 4.3, respectively. The error values are calculated using the standard deviations associated with the measurements. The details of the error calculation is given in Appendix B.

The geometry optimization step provides parameters for making ball bonds with identical BDC and BH for varying σ_N and BT. These bonds, however, have low mechanical strengths due to the minimal use of US.

Table 4.1 BDC (µm) and BH (µm) (shown in italics) at different I_{EFO} and IF combination when σ_N = 80 MPa and BT = 100 ºC (± values are one standard deviation)

I_{EFO} [mA]	IF [mN]	
	350	500
60	42.31 ± 0.47 *11.8 ± 1.0*	47.14 ± 0.97 *7.4 ± 0.9*
70	45.08 ± 0.72 *18.4 ± 1.4*	48.88 ± 0.90 *15.1 ± 0.4*

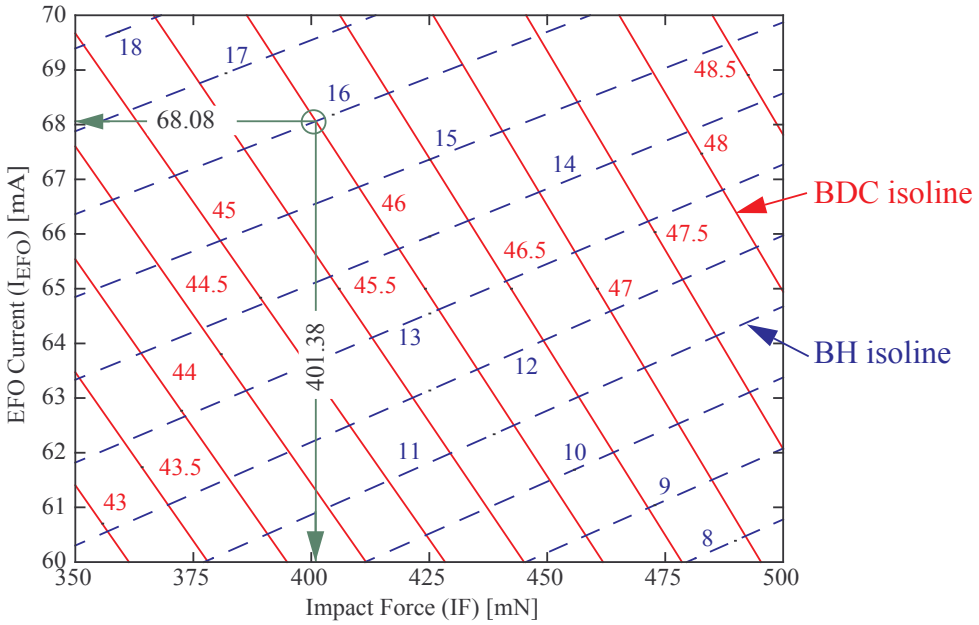

Fig. 4.1 Contour plot of BDC (red solid line) and BH (blue dashed line) used for optimizing bond geometry at σ_N = 80 MPa and BT = 100 ºC. Intersection between target BDC (46 µm) and BH (16 µm) gives IF^{Opt} and I_{EFO}^{Opt} parameters, at minimal US of 11.14 %.

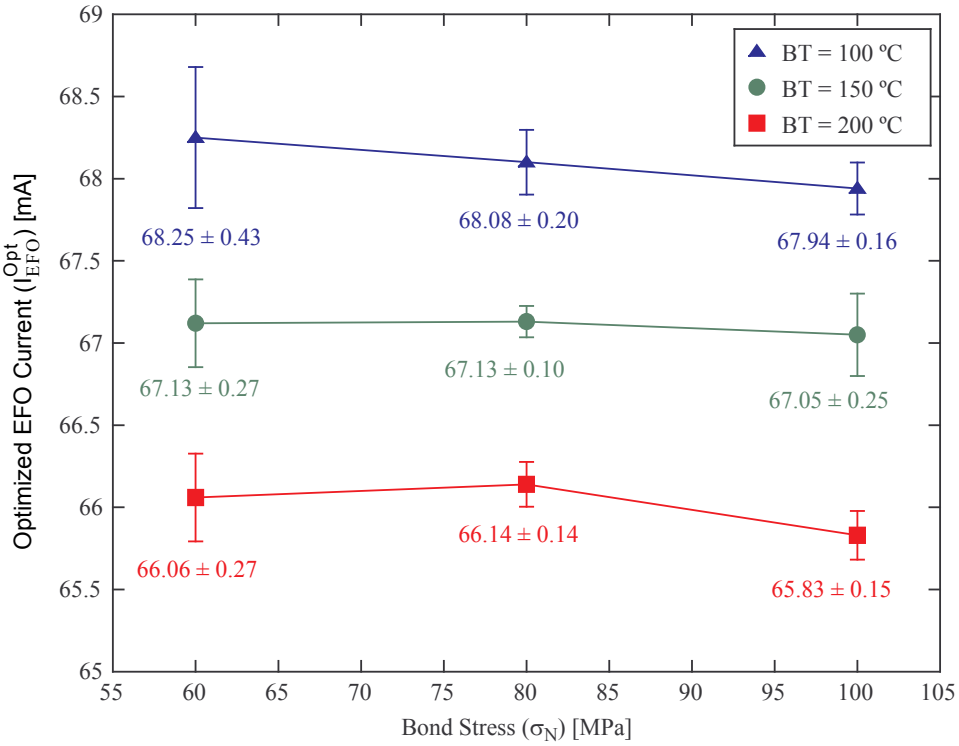

Fig. 4.2 Plot showing I_{EFO}^{Opt} plotted against σ_N for three different BT.

4.2. Verification of Bond Geometry Parameters

Ball bonds are made with optimized I_{EFO} and IF to verify the parameters. BDC and BH of each bond are measured and the average values with one standard deviation are given in Table 4.2. The measured values are within the acceptable range of the target values. Hence, the I_{EFO}^{Opt} and IF^{Opt}

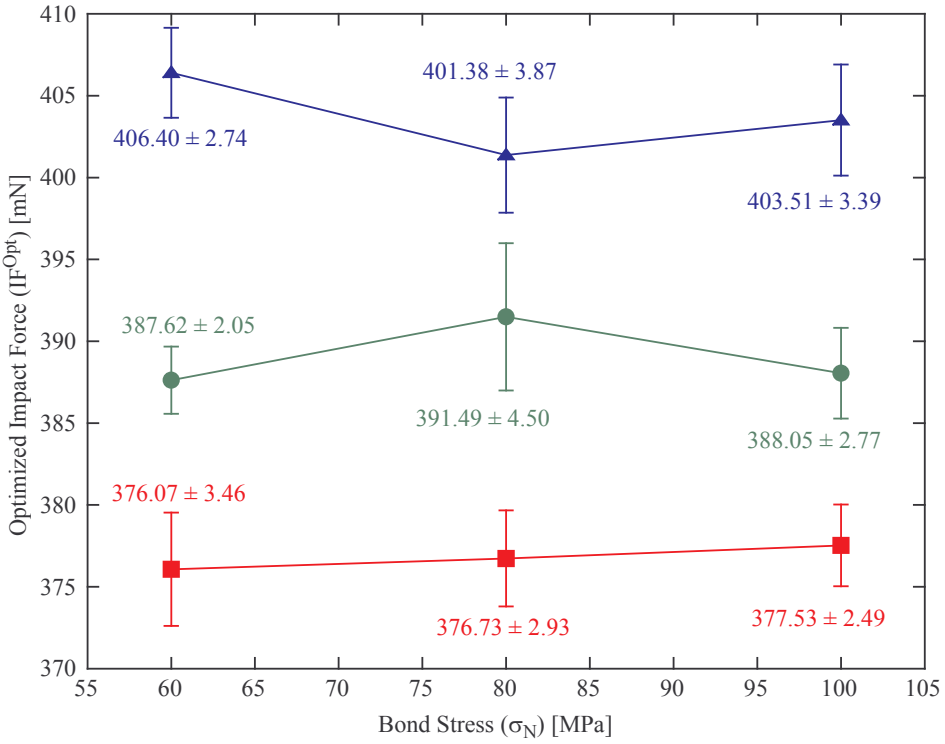

Fig. 4.3 Plot showing IF^{Opt} plotted against σ_N for three different BT. The legends are same as Fig. 4.2.

Table 4.2 BDC [µm] and BH [µm] (shown in italics) of ball bonds at different σ_N and BT combination after geometry optimization (± values are one standard deviation)

BT [ºC]	σ_N [MPa]		
	60	80	100
100	45.92 ± 0.30 *16.3 ± 0.2*	45.88 ± 1.09 *16.4 ± 0.2*	46.07 ± 0.84 *16.0 ± 0.6*
150	46.13 ± 0.77 *16.0 ± 0.4*	46.08 ± 0.54 *16.3 ± 0.4*	46.28 ± 0.24 *15.6 ± 0.4*
200	46.17 ± 0.22 *15.8 ± 0.4*	46.12 ± 0.76 *16.2 ± 0.2*	46.40 ± 0.37 *15.6 ± 0.8*

values obtained from the geometry optimization step are considered adequate to proceed to the next step of the study.

4.3. Bond Strength Optimization

Bond strength values are optimized by increasing the US from the minimal levels with 1 % increment until UED is detected through the bonder microscope. Ball bonds deviate from the target geometry values when UED starts occurring. The BDC and BH values of each bond are measured, and then the bonds are sheared towards the wedge bond.

The BDC and BH values as a function of US are shown in Fig. 4.4. The SF and SS values are plotted against the respective US levels in Fig. 4.5. The US required to obtain the final BDC (BDC_{final}) value of 46.5 µm is chosen as optimum US (US_{Opt}^{interp}) by interpolation. The BDC_{final} is chosen with an additional UED of 0.5 µm, because a small amount of UED is proven to be beneficial for bond quality and process robustness [35]. Using the US_{Opt}^{interp}, corresponding SS values are interpolated from the plots. These values are considered the optimum SS (SS_{Opt}^{interp}) for the ball bonds. The US_{Opt}^{interp} and SS_{Opt}^{interp} values are given in Fig. 4.5b, Fig. 4.5d, and Fig. 4.5f.

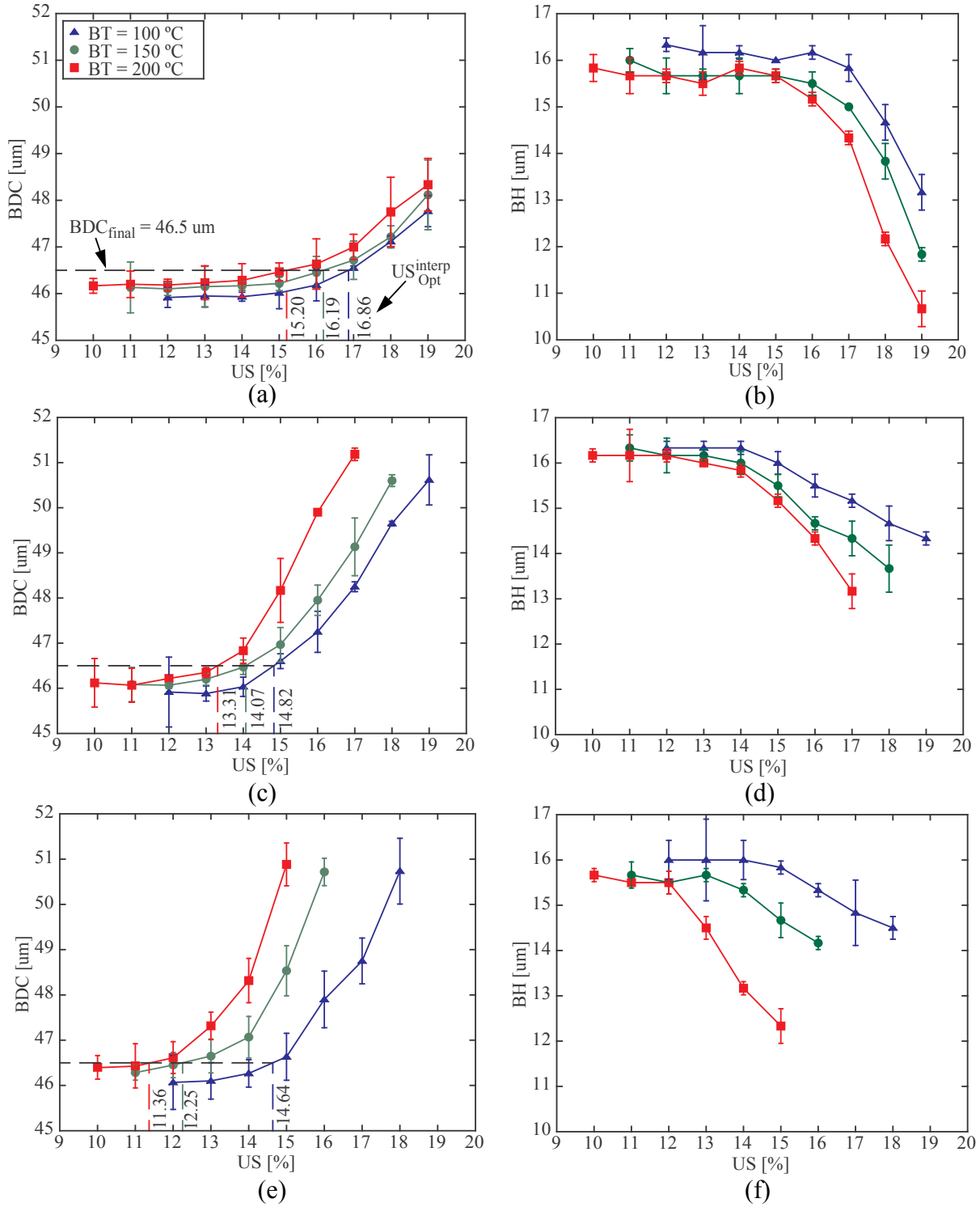

Fig. 4.4 Plots showing BDC and BH at, (a) and (b) for σ_N = 60 MPa, (c) and (d) for σ_N = 80 MPa, (e) and (f) for σ_N = 100 MPa, respectively, for three different BT. The horizontal dashed line represents the BDC_{final} which is used to interpolate the US_{Opt}^{interp} from experimental results. The vertical dashed lines shows US_{Opt}^{interp} values for different BT.

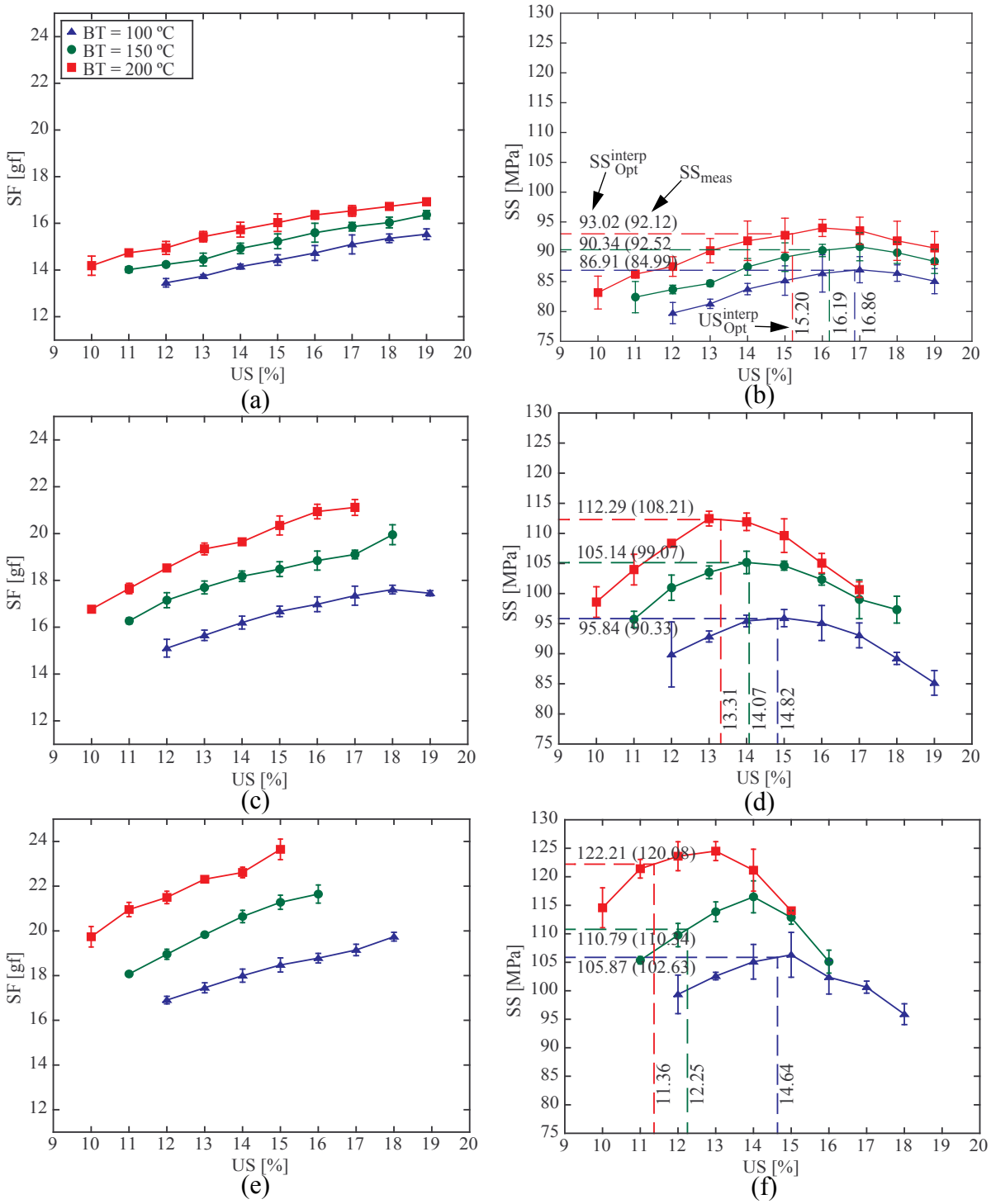

Fig. 4.5 Plots showing SF and SS at, (a) and (b) for σ_N = 60 MPa, (c) and (d) for σ_N = 80 MPa, (e) and (f) for σ_N =100 MPa, respectively, for three different BT. The US_{Opt}^{interp} lines from Fig. 4.4 are used to identify SS_{Opt}^{interp} from SS plots using interpolation. The vertical dashed lines show the SS_{Opt}^{interp} values with the SS values measured from verification bonds, SS_{meas}, in parentheses

4.4. Verification of Optimized Parameters

Test bonds are made with each set of optimized parameters for verification purpose. The bond geometry are measured first, and then the bonds are sheared. The average BDC, BH, and SS values with one standard deviation are shown in Table. 4.3. The maximum SS for ball bonds are achieved when both the σ_N and BT are at the highest. The trend in resultant SS agree with the interpolated SS (SS_{Opt}^{interp}) values from the bond strength optimization step. The maximum deviation between the measured and interpolated SS results is 5.8 % which can be attributed to the sample-to-sample variation.

SEM images of typical optimized bonds are shown in Fig. 4.6 as a function of σ_N and BT. The images represent the center and corner points of the BT-BS DOE. Minor Al splash is observed for all the ball bonds. The neck area for the low BT (100 ºC) bonds are bigger compare to the higher BT bonds.

Table 4.3 BDC [µm], BH [µm], and SS [MPa] of ball bonds for different σ_N and BT combination after geometry optimization (± values are one standard deviation)

BT [ºC]	Responses	σ_N [MPa]		
		60	80	100
100	BDC	46.13 ± 0.17	46.26 ± 0.10	46.12 ± 0.15
	BH	16.6 ± 0.3	16.5 ± 0.4	16.5 ± 0.3
	SS	84.99 ± 0.93	90.33 ± 0.69	102.63 ± 0.62
150	BDC	46.45 ± 0.20	46.27 ± 0.17	46.36 ± 0.40
	BH	16.2 ± 0.2	16.6 ± 0.2	15.8 ± 0.3
	SS	92.52 ± 1.18	99.07 ± 1.31	110.34 ± 1.57
200	BDC	46.55 ± 0.29	46.81 ± 0.23	46.49 ± 0.22
	BH	16.4 ± 0.4	16.5 ± 0.2	16.7 ± 0.2
	SS	92.12 ± 0.84	108.21 ± 1.47	120.08 ± 1.23

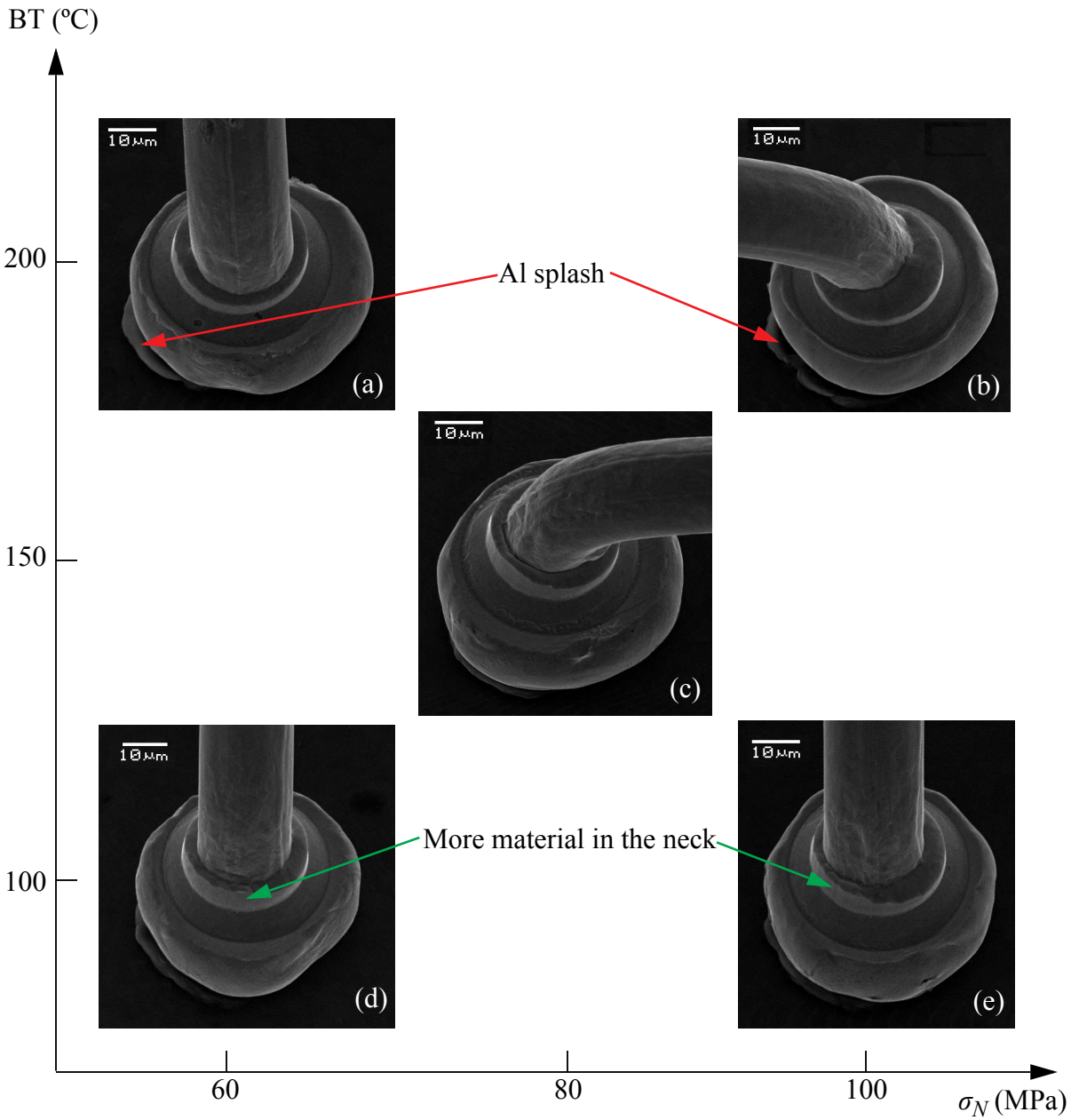

Fig. 4.6 SEM images of optimized 20 µm diameter PCS wire ball bonds as function of σ_N and BT. All the images are taken at a 30 ºC angle from horizontal.

5. Discussion

5.1. Effect of Bond Stress and Temperature on Geometry

Minor variations exist in the I_{EFO} and IF values across the σ_N, which are the two key parameters responsible for the initial geometry formation. The average difference between the I_{EFO} values for the 60 and 100 MPa of σ_N is 0.31 %. The difference is even smaller (0.09 %) for the IF values. The overlapping errorbars in Fig. 4.2 and Fig. 4.3 suggest that the existent variations for a given BT is due to the uncertainty associated with the experiments. The EFO-IF DOE is executed before BF is enabled which means ball bonds are influenced less by the BF during initial bond formation. Thus, it can be conferred that the bond geometry formation is not significantly influenced by the σ_N. This finding, however, does not agree with the studies reported on the effect of bond force on Au ball bonds [42,43].

A bonding model for bonding force is proposed based on the experimental results in [42]. The model suggests that the bonded area at the interface between Au ball bond and bonding pad should increase with the increased bond force. The increased bond force would make the bonds grow outwards resulting in larger BDC. The study presented in [43] confers that the ball bonds change from elastic condition to plastic condition when bond force increases from very low to very high. The contact area increases during the plastic deformation and larger ball bonds form when the bond force is high.

One reason for PCS ball bonds behaving differently to σ_N compared to Au ball bonds could be attributed to the range of σ_N used in this study. An empirical study on Cu ball bonds in [45] shows that the bond geometry does not get affected by σ_N when it is varied between ~103 and ~160 MPa. However, Cu ball bonds have smaller BDC and higher BH when the σ_N is lower than 100 MPa. The BDC increases and BH decreases once the σ_N value is increased above 160 MPa. Similarly, the influence of BF on PCS ball bonds could be insignificant within the chosen range of σ_N (60 to 100 MPa).

The geometry formation is significantly influenced by the BT unlike the σ_N. On average 3.16 % more I_{EFO} and 7.16 % more IF are required to form similar bonds when the BT decreases from

200 to 100 ºC. The results mean larger FAB (due to larger I_{EFO}), and subsequently more force is required when lower temperature is used to achieve the target BDC and BH.

The higher temperature at the bond interface heats up the wire material during bonding. Hence, the tails forming during high temperature ball-wedge bonding is softer. In addition, the FABs become more deformable due to higher bond interface temperature. Hence, the target geometry is possible to achieve with smaller FABs and lower IF for the high BT process. Similar effect of temperature on Cu ball bond is reported in [45]. In [45], bond temperature is varied from 25 to 220 ºC while other bonding parameters were kept unchanged. The study found that the bond diameter increases by ~6.1 % while the height decreases by ~6.0 % due to the temperature increase.

Stronger adhesion is observed at the bond interface when higher temperature is used [1,39]. The elevated temperature increases internal energy, improves atomic diffusion, and solubility of the metals at the interface. Hence, stronger influence of US is required to prevent NSOP when the BT is low. The frictional energy generated by higher US compensates the lower substrate BT. Hence, the US_{min} required during geometry optimization is higher for lower BT process. The BT = 100 ºC process requires ~20.8 % more US_{min} to prevent the NSOP compared to the BT = 200 ºC process.

5.2. Effect of Bond Stress and Temperature on Bond Strength

The US values are responsible for the strengthening of the bonds and the optimized US values get effected significantly by the σ_N and BT. For a given σ_N, larger SS is obtained with lower amount of US when the BT is higher. For example, when σ_N = 60 MPa, ball bonds made at 200 ºC achieve 7.03 % more SS than 100 ºC bonds, even though 10.92 % less US is used on the 200 ºC bonds. The significant improvement of shear force due to increased temperature is observed on Au ball bonds [40,41]. In [41], the average shear strength of Au ball bonds increased by ~24.1 % when the process temperature is increased from 100 to 200 ºC. The results suggest that PCS ball bonds respond to temperature change in a way similar to the Au ball bonds.

The SS of ball bonds increase when the σ_N is increased with BT kept unchanged. For example, 8.83 % more SS is achieved with 17.17 % less US when BT = 200 ºC, but σ_N changed from 80 to 100 MPa. The result agrees with the existing literature which used Au ball bonds to study the effect of bond force on bond strength [41-44]. The interfacial contact between a ball bond and a bond pad increases when the BF (or σ_N) is increased and stronger bonds form due to larger inter-facial contact. As a result, the PCS ball bonds show increased SS when the σ_N is increase from 60 to 100 MPa.

The effect of σ_N and BT on bond strengths is represented in a contour plot in Fig. 5.1. The plot shows the interaction between the $\mathrm{US}_{\mathrm{Opt}}^{\mathrm{interp}}$ and $\mathrm{SS}_{\mathrm{Opt}}^{\mathrm{interp}}$ by plotting them against the BT and σ_N. The overlapping lines are isolines for constant $\mathrm{US}_{\mathrm{Opt}}^{\mathrm{interp}}$ and resultant $\mathrm{SS}_{\mathrm{Opt}}^{\mathrm{interp}}$. From the plot, a process zone of high σ_N and high BT found to result in SS > 120 MPa is identified. The plot suggests that the lower amount of US is sufficient to achieve higher SS since both high BT and high σ_N increases the shear force of the bonds. This optimum process zone is located at the corner of the σ_N and BT DOE which makes it harder to identify a process window for the PCS bonds. The process window seems to be located outside of the DOE where σ_N and BT values are higher than the maximum values of DOE.

The $\mathrm{US}_{\mathrm{Opt}}^{\mathrm{interp}}$ for different σ_N and BT is calculated using the geometric constraint in this study. However, it should be noted that the increment of US keeps strengthening the ball bonds as shown in Fig. 4.5a, Fig. 4.5c, and Fig. 4.5e. The shear force (SF) of ball bonds keep increasing as the US

is increased gradually from the US_{min} level. Instead of using target BDC, it would have been reasonable to choose the optimum US values as the ones that would result in the highest SFs. The problem with that is the bond strength values would have been no longer comparable among the different σ_N and BT combinations. The bonded area among the ball bonds would be different since different amount of UED would be present at each bonds. The methodology presented in this study keeps the geometry constrain and normalizes the SF to SS values. In consequence the bond contact area remains similar and the calculated US_{Opt}^{interp} values become comparable among different combinations of σ_N and BT.

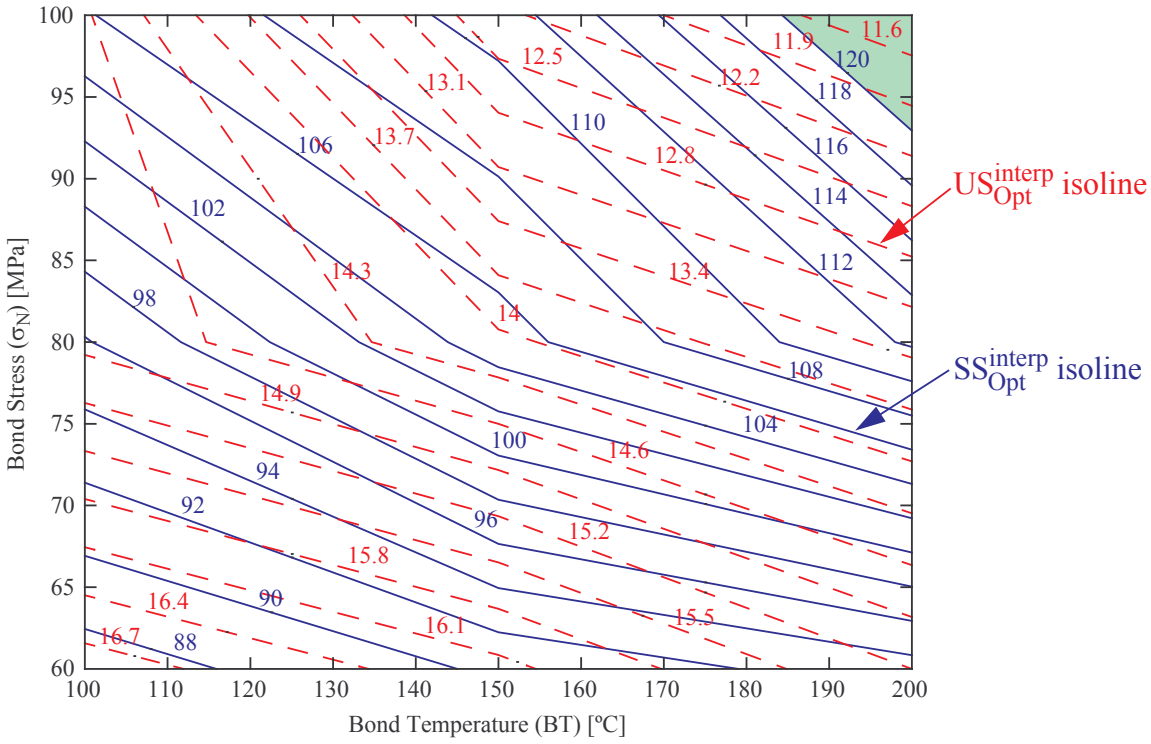

Fig. 5.1 Contour plot showing the interaction between US_{Opt}^{interp} (red dashed line) and SS_{Opt}^{interp} (blue solid line) for BDC_{final} = 46.5 µm. The shaded region (in green) indicates the combination of σ_N =60 MPa and BT =200 ºC resulting in SS > 120 MPa.

5.3. Effect of UED on Ball Bonds

The US_{Opt}^{interp} for this study is calculated using an additional UED value of 0.5 µm added to the target BDC of 46 µm. The US_{Opt}^{interp} is dependent on this UED value and it is possible to evaluate the trend of US_{Opt}^{interp} against UED. The US_{Opt}^{interp} and the corresponding SS_{Opt}^{interp} are plotted against the UED value ranging from 0 µm to 2 µm in Fig. 5.2. The US_{Opt}^{interp} value increases sharply from the US_{min} value initially and then steadily increases as the UED value increases. The result also quantifies the additional US that would be required to control the UED in ball bonds for specific process condition. For example, 16.8 % US is required for a final BDC of 47 µm (46 µm BDC with UED value of 1 µm) when σ_N = 60 MPa and BT = 200 ºC.

The corresponding SS_{Opt}^{interp} follows a different trend to the incrementing UED values. The SS_{Opt}^{interp} keeps increasing until it peaks at a critical UED value, then gradually decreases. This result is important because it shows that the bond SS can not be maximized with US beyond a critical UED value. The effect of σ_N and BT on US_{Opt}^{interp} and SS_{Opt}^{interp}, however, maintains a similar trend discussed in the previous section irrespective of the UED value.

The results also show that bonds made at higher BT values require lesser amount of UED to achieve high SS in contrast to the lower BT bonds. The SS values of lower BT bonds are lower than the higher BT bonds irrespective of the amount of UED added. UED seems beneficial to the SS at 150 and 200 ºC as it increases the SS values by 5 to 10 MPa. However, UED increases the SS of 100 ºC bonds by less than 2 to 3 MPa. Hence, the UED is not quite beneficial when the BT is low.

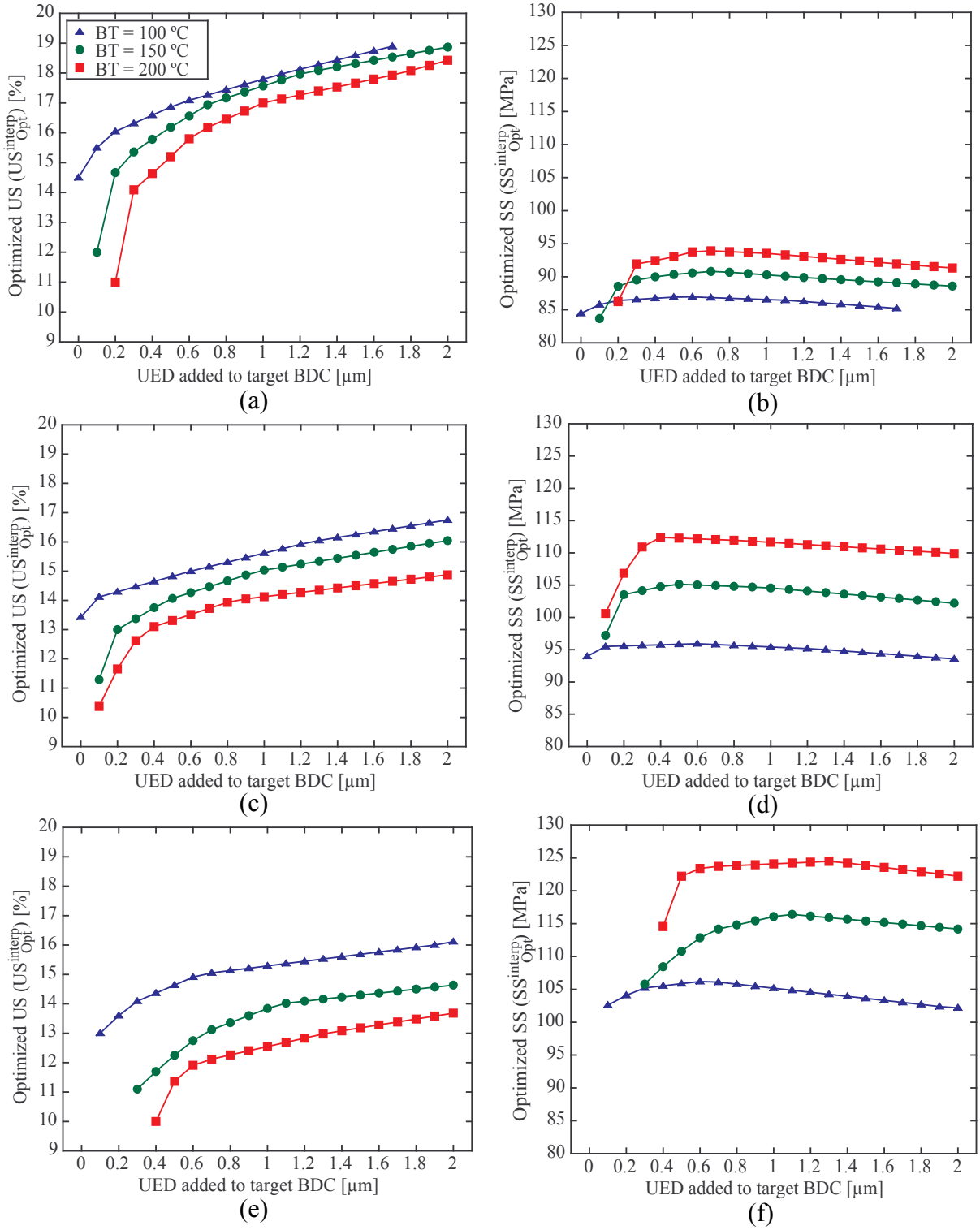

Fig. 5.2 Plots showing US^{interp}_{Opt} and SS^{interp}_{Opt} at (a) and (b) for σ_N = 60 MPa, (c) and (d) for σ_N = 80 MPa, and (e) and (f) for σ_N = 100 MPa, respectively, for three different BT.

6. Conclusions

The study identifies an optimal process condition for 20 µm PCS wire ball bonds. The ball bonds made with this optimized parameters achieve the acceptable geometry and strength. The results show that high bond stress and process temperature is required to form ball bonds with sufficient strength. The ultrasound required at the optimal process condition is comparatively low which could be beneficial for sensitive devices.

The methodology used to study the bondability of PCS ball bonds is designed to be fast and requires minimal amount of resources. The experimental procedure is flexible and each step of the process can be modified independently to improve the process. This methodology can be adapted to study the bondability of other bonding wire materials promptly.

The study have found optimum process settings for PCS ball bonds. However, the process window has not been characterized in this study. In case of any process optimization, the size of the process window is of interest. The target values are maintained with the specified tolerances inside the process window. The next step of the study needs to include the process window characterization.

The optimized PCS ball bonds are not verified for long-term reliability in this study. The future steps would include assessing the reliability of PCS ball bonds for each combination of bond stress and temperature using standardized reliability testing. The reliability of the wedge bonds need to be assessed as well. In order for the PCS wire to be fully acceptable in the volume production, wedge bond optimization and overall reliability assessment is required.

References

[1] Harman, George G. Wire bonding in microelectronics. McGraw-Hill, 2010.

[2] Chauhan, Preeti S., Anupam Choubey, ZhaoWei Zhong, and Michael G. Pecht. Copper wire bonding. Springer New York, 2014.

[3] Lu, Charlie. "Review on silver wire bonding." In Microsystems, Packaging, Assembly and Circuits Technology Conference (IMPACT), 2013 8th International, pp. 226-229. IEEE, 2013.

[4] Handbook, A. S. M. "Vol. 2, 1990." Properties & Selection: Nonferrous Alloys and Special Purpose Materials, ASM International, Materials Park, OH.

[5] Guojun, Hu. "Comparison of copper, silver and gold wire bonding on interconnect metallization." In Electronic Packaging Technology and High Density Packaging (ICEPT-HDP), 2012 13th International Conference on, pp. 529-533. IEEE, 2012.

[6] Yoo, Kyung-Ah, Chul Uhm, Tae-Jin Kwon, Jong-Soo Cho, and Jeong-Tak Moon. "Reliability study of low cost alternative Ag bonding wire with various bond pad materials." In Electronics Packaging Technology Conference, 2009. EPTC'09. 11th, pp. 851-857. IEEE, 2009.

[7] Cho, Jong-Soo, Kyeong-Ah Yoo, Sung-Jae Hong, Jeong-Tak Moon, Yong-Je Lee, Wongil Han, Hanki Park et al. "Pd effects on the reliability in the low cost Ag bonding wire." In Electronic Components and Technology Conference (ECTC), 2010 Proceedings 60th, pp. 1541-1546. IEEE, 2010.

[8] Cho, Jong-Soo, Hee-Suk Jeong, Jeong-Tak Moon, Se-Jin Yoo, Jae-Seok Seo, Seung-Mi Lee, Seung-Weon Ha, Eun-Kyu Her, Suk-Hoon Kang, and Kyu-Hwan Oh. "Thermal reliability & IMC behavior of low cost alternative Au-Ag-Pd wire bonds to Al metallization." In Electronic Components and Technology Conference, 2009. ECTC 2009. 59th, pp. 1569-1573. IEEE, 2009.

[9] Guo, Rui, Tao Hang, Dali Mao, Ming Li, Kaiyou Qian, Zhong Lv, and Hope Chiu. "Behavior of intermetallics formation and evolution in Ag–8Au–3Pd alloy wire bonds." Journal of Alloys and Compounds 588 (2014): 622-627.

[10] Wu, Jie, Jeong-Ho Yang, Oranna Yauw, Ivy Qin, Tom Rockey, and Bob Chylak. "Study of 0.6 mil silver alloy wire in challenging bonding processes." In Electronics Packaging Technology Conference (EPTC), 2014 IEEE 16th, pp. 472-476. IEEE, 2014.

[11] Cheng, C. H., H. L. Hsiao, S. I. Chu, Y. Y. Shieh, C. Y. Sun, and Chao Peng. "Low cost silver alloy wire bonding with excellent reliability performance." In Electronic Components and Technology Conference (ECTC), 2013 IEEE 63rd, pp. 1569-1573. IEEE, 2013.

[12] Jang, You Cheol, So Yeon Park, Hyoung Dong Kim, Yeo Chan Ko, Kyo Wang Koo, Mi Ri Choi, Hyung Giun Kim et al. "Study of intermetallic compound growth and failure mechanisms in long term reliability of silver bonding wire." In Electronics Packaging Technology Conference (EPTC), 2014 IEEE 16th, pp. 704-708. IEEE, 2014.

[13] Chuang, Tung-Han, Che-Cheng Chang, Chien-Hsun Chuang, Jun-Der Lee, and Hsing-Hua Tsai. "Formation and growth of intermetallics in an annealing-twinned Ag-8Au-3Pd wire bonding package during reliability tests." Components, Packaging and Manufacturing Technology, IEEE Transactions on 3, no. 1 (2013): 3-9.

[14] Cho, Jong-Soo, Kyung-Ah Yoo, Jeong-Tak Moon, Seoung-Bum Son, Se-Hee Lee, and Kyu Hwan Oh. "Pd effect on reliability of Ag bonding wires in microelectronic devices in high-humidity environments." Metals and Materials International 18, no. 5 (2012): 881-885.

[15] Tanna, Suresh, Jairus L. Pisigan, W. H. Song, Cristopher Halmo, John Persic, and Michael Mayer. "Low cost Pd coated Ag bonding wire for high quality FAB in air." In Electronic Components and Technology Conference (ECTC), 2012 IEEE 62nd, pp. 1103-1109. IEEE, 2012.

[16] Gomes, J., M. Mayer, and B. Lin. "Development of a fast method for optimization of Au ball bond process." Microelectronics Reliability 55, no. 3 (2015): 602-607.

[17] McKenna, Robert G., and Richard L. Mahle. "High impact bonding to improve reliability of VLSI die in plastic packages." In Electronic Components Conference, 1989. Proceedings., 39th, pp. 424-427. IEEE, 1989.

[18] Toyozawa, Kenji, Kazuya Fujita, Syozo Minamide, and Takamichi Maeda. "Development of copper wire bonding application technology." Components, Hybrids, and Manufacturing Technology, IEEE Transactions on 13, no. 4 (1990): 667-672.

[19] Schwizer, Jürg, Michael Mayer, and Oliver Brand. Force sensors for microelectronic packaging applications. Springer Science & Business Media, 2006.

[20] Gaul, Holeger, Martin Schneider-Ramelow, Klaus-Dieter Lang, and Herbert Reichl. "Predicting the shear strength of a wire bond using laser vibration measurements." In Electronics Systemintegration Technology Conference, 2006. 1st, vol. 2, pp. 719-725. IEEE, 2006.

[21] Small Precision Tools Inc., “Basics of Ball Bonding”, In: Technical Guide for Bonding Capillaries. Available online at: http://www.smallprecisiontools.com/index.cfm?parents_id=563.

[22] Di Erick Xu, Jimy Gomes, Michael Mayer, Rob Lyn, John Persic. “Thermal Aging Behavior of Fine Pitch Palladium Coated Silver (PCS) Ball Bonds on Al Metallization.” In International Microelectronics Assembly and Packaging Society (IMAPS), 2015 48th, IMAPS, 2015.

[23] Chen, QiJia, Ariel Pagba, Dexter Reynoso, and Sven Thomas. "Cu wire and beyond-Ag wire an alternative to Cu?." In Electronics Packaging Technology Conference (EPTC), 2010 12th, pp. 591-596. IEEE, 2010.

[24] Chang, Hen-So, Ker-Chang Hsieh, Theo Martens, and Albert Yang. "The effect of Pd and Cu in the intermetallic growth of alloy Au wire." Journal of electronic materials 32, no. 11 (2003): 1182-1187.

[25] Lin, J. C., and J. Y. Chan. "On the resistance of silver migration in Ag-Pd conductive thick films under humid environment and applied dc field." Materials Chemistry and Physics 43, no. 3 (1996): 256-265.

[26] MIL-STD-883E: Bond Strength (destructive bond pull test), METHOD 2011.7 (1989), pp.1-6.

[27] Electronic Industries Alliance; “EIA/JEDEC Standard. Wire Bond Shear Test method. EIA/JESD22-B116A”, August 2009. USA.

[28] Pequegnat, Andrew. "A Study of the Electrical Flame Off Process During Thermosonic Wire Bonding with Novel Wire Materials." (2010).

[29] Nguyen, Luu T., David McDonald, Anselm R. Danker, and Peter Ng. "Optimization of copper wire bonding on Al-Cu metallization." Components, Packaging, and Manufacturing Technology, Part A, IEEE Transactions on 18, no. 2 (1995): 423-429.

[30] Sheaffer, Michael, Lee R. Levine, and Brian Schlain. "Optimizing the wire-bonding process for copper ball bonding, using classic experimental designs." Components, Hybrids, and Manufacturing Technology, IEEE Transactions on 10, no. 3 (1987): 321-326.

[31] Qian, Qiuxiao, Yong Liu, Timwah Luk, and Scott Irving. "Wire bonding capillary profile and bonding process parameter optimization simulation." In Thermal, Mechanical and

Multi-Physics Simulation and Experiments in Microelectronics and Micro-Systems, 2008. EuroSimE 2008. International Conference on, pp. 1-7. IEEE, 2008.

[32] Sheaffer, Michael, Lee R. Levine, and Brian Schlain. "Optimizing the wire-bonding process for copper ball bonding, using classic experimental designs." Components, Hybrids, and Manufacturing Technology, IEEE Transactions on 10, no. 3 (1987): 321-326.

[33] Yeh, Jun-Hsien, and Tsung-Nan Tsai. "Optimizing the fine-pitch copper wire bonding process with multiple quality characteristics using a grey-fuzzy Taguchi method." Microelectronics Reliability 54, no. 1 (2014): 287-296.

[34] Tsai, Tsung-Nan. "A hybrid intelligent approach for optimizing the fine-pitch copper wire bonding process with multiple quality characteristics in IC assembly." Journal of Intelligent Manufacturing 25, no. 1 (2014): 177-192.

[35] Gomes, J., Mayer, M. “Effect of Au Ball Bond Geometry on Bond Strength and Process Parameters, and Assessing Reliability on Al Bond Pad using Integrated Stress Sensors.” In Electronic Components and Technology Conference (ECTC), 2015 IEEE 65th, IEEE, 2015

[36] McCracken, Michael James, Yasumasa Koda, Hyoung Joon Kim, Michael Mayer, John Persic, June Sub Hwang, and Jeong-Tak Moon. "Explaining Nondestructive Bond Stress Data From High-Temperature Testing of Au-Al Wire Bonds." Components, Packaging and Manufacturing Technology, IEEE Transactions on 3, no. 12 (2013): 2029-2036.

[37] Shah, A., M. Mayer, Y. Zhou, J. Persic, and J. T. Moon. "Optimization of ultrasound and bond force to reduce pad stress in thermosonic Cu ball bonding." In Electronics Packaging Technology Conference, 2009. EPTC'09. 11th, pp. 10-15. IEEE, 2009.

[38] “ESEC launches wire bonder with more speed and precision”, EEtimes News & Analysis, Sep. 15, 1999.

[39] Breach, C. D., and F. W. Wulff. "A brief review of selected aspects of the materials science of ball bonding." Microelectronics Reliability 50, no. 1 (2010): 1-20.

[40] Weiner, J. A., G. V. Clatterbaugh, H. K. Charles Jr, and B. M. Romenesko. "Gold ball bond shear strength: effects of cleaning, metallization, and bonding parameters." In Proc. IEEE 33rd Electronic Components Conference. Orlando, Florida, USA, pp. 208-220. 1983.

[41] Hu, Shze J., G. E. Lim, Thiam L. Lim, and Kar P. Foong. "Study of temperature parameter on the thermosonic gold wire bonding of high-speed CMOS." Components, Hybrids, and Manufacturing Technology, IEEE Transactions on 14, no. 4 (1991): 855-858.

[42] Xu, Hui, Changqing Liu, Vadim V. Silberschmidt, Zhong Chen, and Jun Wei. "Initial bond formation in thermosonic gold ball bonding on aluminium metallization pads." Journal of Materials Processing Technology 210, no. 8 (2010): 1035-1042.

[43] Qi, Jun, Ngar Chun Hung, Ming Li, and Deming Liu. "Effects of process parameters on bondability in ultrasonic ball bonding." Scripta materialia 54, no. 2 (2006): 293-297.

[44] Jeng, Yeau-Ren, and Jeng-Nan Lin. "Study of interfacial phenomena affecting thermosonic wire bonding in microelectronics." Journal of tribology 125, no. 3 (2003): 576-581.

[45] Xu, Hui, Changqing Liu, Vadim V. Silberschmidt, and Honghui Wang. "Effects of process parameters on bondability in thermosonic copper ball bonding." In Electronic Components and Technology Conference, 2008. ECTC 2008. 58th, pp. 1424-1430. IEEE, 2008.

Appendix A. MATLAB Script for Generating Contour Plots

The following MATLAB script is developed to calculate the optimized parameters for the bond geometry formation.

The filename is “DOE_Complete_Program.m”

```
%{
Author: Jimy Gomes
Purpose:
The code generates the controur plot from the given inputs. The input values
are
obtained from experiments using either a 2x2 or a 3x3 DOE. The code is used to
calculate
the optimized parameters automatically for the target BDC and BH values.
The optimized parameters are displayed on the MATLAB command window and
identified on the plot.
%}

clear all;
close all;
clc;

%Choosing between 2x2 or 3x3 DOE
n=input('Press 3 for 3x3 DOE, 2 for 2x2 DOE = ');

%DOE Data Input

IF=[];
disp('Insert IF values from lowest to highest');
for i=1:n;
    a=['IF',num2str(i),' = '];
    IF(i)=input(a);
end

I_EFO=[];
disp('Insert I_EFO values from lowest to highest');
for i=1:n;
    a=['I_EFO',num2str(i),' = '];
    I_EFO(i)=input(a);
end
```

```
BDC=[];
for i=1:n;
   for j=1:n;
       a=['Average BDC from IF ',num2str(IF(i)),' and I_EFO
',num2str(I_EFO(j)),' = '];
       BDC(j,i)=input(a);
   end
end

BH=[];
for i=1:n;
   for j=1:n;
       a=['Average BH from IF ',num2str(IF(i)),' and I_EFO
',num2str(I_EFO(j)),' = '];
       BH(j,i)=input(a);
   end
end

%Contour plot generator

figure(1)

[hCont1,h1]=contour('v6',IF,I_EFO,BDC,'r');    %'v6' allows to plot to be
captured by 'plot2mif' function
hold on;
[hCont2,h2]=contour('v6',IF,I_EFO,BH,'b');

set(h1,'Linestyle','-');
set(h2,'Linestyle','--');

clabel(hCont1,'FontSize',10,'Color','r');
clabel(hCont2,'FontSize',10,'Color','b');
set(gca,'box','on');

xlabel('IF [mN]');
ylabel('I_E_F_O [mA]');

%DOE Location

for i=1:n
    for j=1:n
```

```
        plot(IF(i),I_EFO(j),'ko','markerfacecolor','k');
    end
end
if n==3
    plot([IF(2),IF(2)],[I_EFO(1),I_EFO(3)],'-.','color','k');
    plot([IF(1),IF(3)],[I_EFO(2),I_EFO(2)],'-.','color','k');
end

% Inputting target BDC and BH value

a='Target BDC = ';
BDCtar=input(a);
a='Target BH = ';
BHtar=input(a);

%Optimized Parameter Calculation

hCont3=contourc(IF,I_EFO,BDC,[BDCtar BDCtar]);
hCont4=contourc(IF,I_EFO,BH,[BHtar BHtar]);
hCont3(:,1)=[];
hCont4(:,1)=[];
[IFopt,I_EFOopt]=polyxpoly(hCont3(1,:),hCont3(2,:),hCont4(1,:),hCont4(2,:));

X=['Optimized IF = ',num2str(IFopt)];
disp(X);
X=['Optimized I_EFO = ',num2str(I_EFOopt)];
disp(X);

plot(IFopt,I_EFOopt,'gO','markersize',12,'LineWidth',1);
plot([IF(1),IFopt],[I_EFOopt,I_EFOopt],'-','linewidth',1,'color','m');
plot([IFopt,IFopt],[I_EFOopt,I_EFO(1)],'-','linewidth',1,'color','m');
disp(figure(1));
```

Appendix B. Error Calculation on the Bond Geometry Parameters

The method used in this study to calculate the IF^{Opt} and I_{EFO}^{Opt} from 2×2 DOE is not capable of calculating the error values associated with the optimized parameters. As a result, a method is developed to calculate the associated errors using all the measured values.

The number of total measurements used for each 2×2 DOE is 20. Hence, a total of 5^4 (or 625) combinations of IF^{Opt} and I_{EFO}^{Opt} can be generated from the contour plots if every single measured values are used instead of the average values. It is then possible to calculate the standard deviation and error estimates from those IF^{Opt} and I_{EFO}^{Opt} values. Here,

- n_s = number of measured values = 20
- i = 1,..., 625
- X_i = Set of IF^{Opt} values
- Y_i = Set of I_{EFO}^{Opt} values
- $\overline{X_i}$ = Average of X_i values
- $\overline{Y_i}$ = Average of Y_i values
- σ_{X_i} = Standard deviation of X_i values
- σ_{Y_i} = Standard deviation of Y_i values
- ε_{X_i} = Standard error estimate for X_i = $\dfrac{\sigma_{X_i}}{\sqrt{n_s - 1}}$
- ε_{Y_i} = Standard error estimate for Y_i = $\dfrac{\sigma_{Y_i}}{\sqrt{n_s - 1}}$

The MATLAB script given in this section automatically calculates the error estimates using the aforementioned concept. An example contour plot is shown in Fig. 9.1a for σ_N = 80 MPa and BT = 100 ºC process. Only the target BDC (46 µm) and BH (16 µm) isloines are plotted. Each intersection points of the isolines are shown in Fig. 9.1b along with average of intersection points

(P_{avg}) and optimized values from 2×2 DOE analysis (P_{DOE}) which is obtained using methods presented in Appendix A.

An important thing is that not all of 625 points result in parameter set that fall within the range of σ_N and BT used in the experiment. Those values are discarded which results in fewer than 625 X_i and Y_i combination set. This is one of the reason that contribute to the deviation between P_{avg} and P_{DOE} values. The intersection points along with P_{avg} and P_{DOE} for all the process are shown in Fig. 9.2.

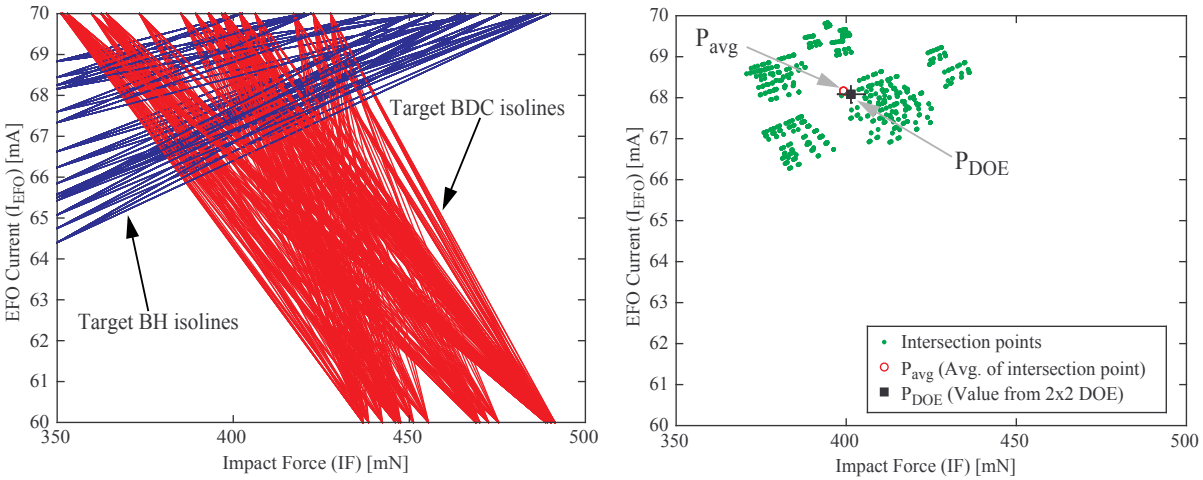

(a) (b)

Fig. 9.1 Plot showing (a) isolines for target BDC (red line) and BH (blue line) values, (b) intersection points of isolines along with average of those points and optimized value obtained from 2×2 DOE analysis. The plots are generated using data obtained from σ_N = 80 MPa and BT = 100 ºC process.

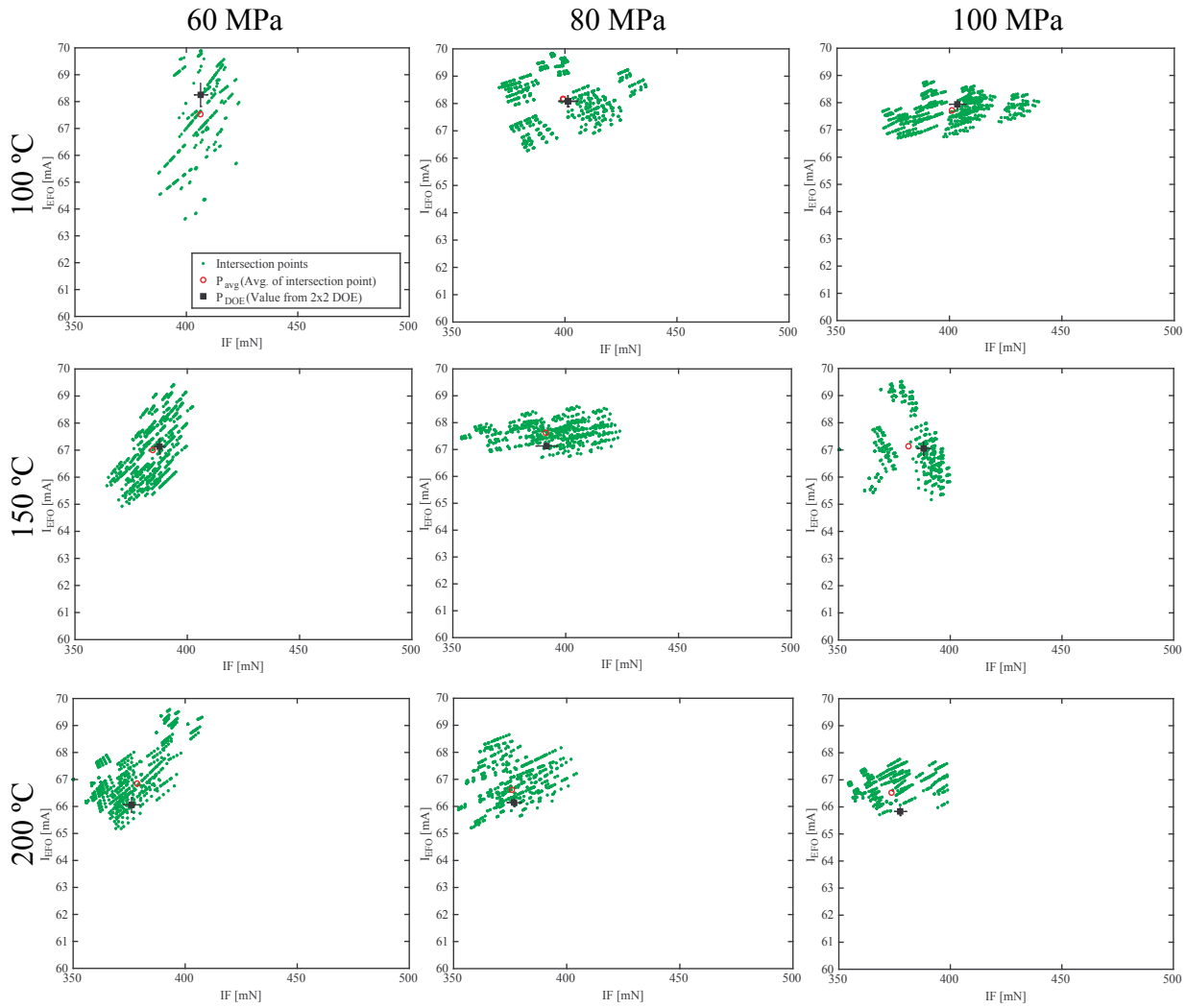

Fig. 9.2 Plot showing intersection points for all the process along with P_{avg} and P_{DOE} values.

The file name is “Contour_plot_error_analysis.m”.

```
%{
Author: Jimy Gomes
Purpose:
The code calculates the standard error associated with the optimized
parameters.
%}


clear all;
close all;
clc;

IF=[350 500]; %x
I_EFO=[60 70]; %y

%BDC Data-Raw
A=[42.52;41.57;42.67;42.12;42.67]; %x1y1
B=[46.87;47.87;46.27;48.42;46.27]; %x2y1
C=[44.37;44.77;45.72;44.57;45.97]; %x1y2
D=[47.52;49.07;49.07;50.02;48.72]; %x2y2

%BH Data-Raw
E=[12.7;10.7;10.7;12.2;12.7]; %x1y1
F=[7.2;7.7;8.7;7.2;6.2]; %x2y1
G=[20.2;16.7;17.2;18.7;19.2]; %x1y2
H=[14.7;14.7;15.7;15.2;15.2]; %x2y2


BDC=[];
BH=[];

BDCtar=46; %Target BDC
BHtar=16;  %Target BH

IFopt=[];
I_EFOopt=[];

X=[]; %IFOpt Matrix
Y=[]; %I_EFOOpt Matrix
```

```
counter=0;

for i=1:length(A)
    for j=1:length(B)
        for k=1:length(C)
            for l=1:length(D)
                BDC(1,1)=A(i,1);
                BDC(1,2)=B(j,1);
                BDC(2,1)=C(k,1);
                BDC(2,2)=D(l,1);

                BH(1,1)=E(i,1);
                BH(1,2)=F(j,1);
                BH(2,1)=G(k,1);
                BH(2,2)=H(l,1);

                figure(1);
                hold on;
                [hCont1,h1]=contour('v6',IF,I_EFO,BDC,[BDCtar,BDCtar],'r');
%               set(hCont1,'color','r');
                [hCont2,h2]=contour('v6',IF,I_EFO,BH,[BHtar,BHtar],'b');
%               set(hCont2,'color','b');

                hCont3=contourc(IF,I_EFO,BDC,[BDCtar,BDCtar]);
                hCont4=contourc(IF,I_EFO,BH,[BHtar,BHtar]);

                if ~isempty(hCont3)
                    if ~isempty(hCont4)
                        hCont3(:,1)=[];
                        hCont4(:,1)=[];

[IFopt,I_EFOopt]=polyxpoly(hCont3(1,:),hCont3(2,:),hCont4(1,:),hCont4(2,:));
                    end
                end

                 if ~isempty(IFopt)
                    if ~isempty(I_EFOopt)
                        X(counter+1,1)=IFopt;
                        Y(counter+1,1)=I_EFOopt;
                    end
```

```
                end

                counter=counter+1;

            end
        end
    end
end

box on;
set(figure(1),'Position',[25   580   560   420]);
xlabel('IF [mN]');
ylabel('I_E_F_O [mA]');

X(X == 0) = []; %removing zero values
Y(Y == 0) = []; %removing zero values

eIF=std(X)/sqrt(length(A)+length(B)+length(C)+length(D)-1); %Standard error
calculation
eIEFO=std(Y)/sqrt(length(A)+length(B)+length(C)+length(D)-1); %Standard error
calculation

X1=['The error values of IF is ', num2str(eIF) ,' mN'];
Y1=['The error values of I_EFO is ', num2str(eIEFO) ,' mA'];

% plot2mif('Erroranalysis_BT_100_BF_133.mif');
clc;

disp(X1);
disp(Y1);

figure(2)
set(figure(2),'Position',[616   582   560   420]);
hold on;

set(gca,'xlim',[350 500],'ylim',[60 70]);
box on;
xlabel('IF [mN]');
ylabel('I_E_F_O [mA]');

avgIF=mean(X);
```

```
avgIEFO=mean(Y);

IFmeas=401.38;                          % Result from 2x2 DOE
IEFOmeas=68.08;                         % Result from 2x2 DOE


X2=['The average value of IF is ', num2str(avgIF) ,' mN'];
Y2=['The average value of I_EFO is ', num2str(avgIEFO) ,' mA'];

disp(X2);
disp(Y2);

plot('v6',X,Y,'g.');
plot('v6',avgIF,avgIEFO,'ro','markersize',4);
plot('v6',IFmeas,IEFOmeas,'ks','markerfacecolor','k','markersize',4);

legend('location','southeast','Intersection points', 'Avg. of intersection
point','Value from 2x2 DOE');

% errorbar('v6',avgIF,avgIEFO,eIEFO,'r');
% herrorbar(avgIF,avgIEFO,eIF,'r');        % Need to download "herrorbar.m"
file from MATLAB forum



errorbar('v6',IFmeas,IEFOmeas,eIEFO,'k');
herrorbar(IFmeas,IEFOmeas,eIF,'k');      % Need to download "herrorbar.m" file
from MATLAB forum


% plot2mif('Errorcloud_BT_100_BF_133.mif');
```